Energy Efficient Data Collection and Device Positioning in UAV-Assisted IoT

Energy Efficient Data Collection and Device Positioning in UAV-Assisted IoT

Zijie Wang, Rongke Liu, *Senior Member, IEEE,* Qirui Liu, John S. Thompson, *Fellow, IEEE,* and Michel Kadoch, *Senior Member, IEEE*

***Abstract*—The Internet-of-Things (IoT) will significantly change both industrial manufacturing and our daily lives. Data collection and three-dimensional (3D) positioning of IoT devices are two indispensable services of such networks. However, in conventional networks, only terrestrial base stations (BSs) are used to provide these two services. On the one hand, this leads to high energy consumption for devices transmitting at cell edges. On the other hand, terrestrial BSs are relatively close in height, resulting in poor performance of device positioning in elevation. Due to their high maneuverability and flexible deployment, unmanned aerial vehicles (UAVs) could be a promising technology to overcome the above shortcomings. In this paper, we propose a novel UAV-assisted IoT network, in which a low-altitude UAV platform is employed as both a mobile data collector and an aerial anchor node to assist terrestrial BSs in data collection and device positioning. We aim to minimize the maximum energy consumption of all devices by jointly optimizing the UAV trajectory and devices' transmission schedule over time, while ensuring the reliability of data collection and required 3D positioning performance. This formulation is a mixed-integer non-convex optimization problem, and an efficient differential evolution (DE) based method is proposed for solving it. Numerical results demonstrate that the proposed network and optimization method achieve significant performance gains in both energy efficient data collection and 3D device positioning, as compared with a conventional terrestrial IoT network.**

***Index Terms*—Internet of Things, unmanned aerial vehicle, data collection, device positioning, differential evolution.**

I. Introduction

THE Internet-of-Things (IoT), which will dramatically change the world by connecting massive number of smart devices to the internet, has received increasing attention from both the professional community and the public. Some research estimated that up to 100 billion IoT devices will be deployed and connected by 2025 [1], ranging from smart watches and entertainment devices for our everyday lives to industrial sensors and actuators for manufacturing [2], [3]. With the continuous improvement of its service coverage and quality, IoT is expected to promote the revolutionary development of many traditional industries including agriculture [4], retail business [5], transportation [6], etc. Despite the enormous application potential and market demand, the existing IoT networks still have some drawbacks, which restrict their further development.

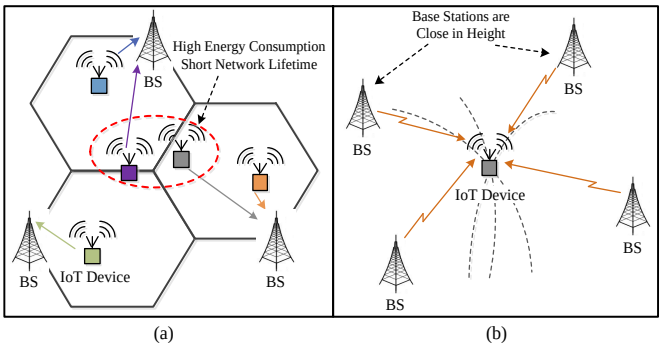

Fig. 1. (a) Data collection and (b) device positioning in conventional terrestrial IoT networks.

The energy consumption of devices is always a major factor limiting the network lifetime, since many devices in IoT are typically required to continuously collect and upload data for more than ten years without recharging [7]. Existing energy-saving technologies reduce the energy consumption of devices by optimizing the sleep schedule or wake-up protocol, such as the extended discontinuous reception (eDRX) and the wake-up signal (WUS) for narrowband internet of things (NB-IoT) [8], [9]. Some recent research pointed out that the transmission energy consumption for the IoT data collection is much higher than for reception [10]. So, optimizing the energy consumption of data collection is believed to be a promising approach to improve the energy efficiency of IoT networks. In order to reduce the energy consumption, it is recommended in [11], [12] that the device delays its data transmission process until the channel quality is good enough to transmit data with relatively low power. However, these approaches are only applicable to a portion of IoT devices with high mobility. In most existing IoT networks, base stations (BSs) are commonly fixed on the ground or buildings, and many devices have very limited mobility, which means that the channel conditions between BSs and devices are unchanged most of the time. Thus, even if the above approaches are applied in the conventional terrestrial IoT network as shown in Fig. 1(a), collecting data from devices at cell edges still requires high energy consumption. Energy efficient data collection in IoT remains an unresolved issue.

Motivated by the explosive growth of the applications requiring location information like mobile marketing and emer-

This work was supported by the Beijing Municipal Science and Technology Project (Z181100003218008).

Z. Wang, R. Liu and Q. Liu are with the School of Electronic and Information Engineering, Beihang University, Beijing 100191, China (e-mail: wangmajie@buaa.edu.cn; rongke_liu@buaa.edu.cn).

J. S. Thompson is with the Institute for Digital Communications, School of Engineering, University of Edinburgh, King's Buildings, Edinburgh, EH9 3JL, U.K. (e-mail: john.thompson@ed.ac.uk).

M. Kadoch is with the Department of Electrical Engineering, École de Technologie Supérieure, University of Quebec, Montreal, QC H3C 1K3, Canada (e-mail: michel.kadoch@etsmtl.ca).

gency services [13], device positioning has been considered as an enabling technology and essential service for future IoT networks [14]. There are some existing technologies which have the capability of device positioning, including the Global Navigation Satellite Systems (GNSS) positioning [15], the positioning technologies using multiple-input-multiple-output systems (referred to below as "MIMO positioning") and the observed time difference of arrival (OTDoA) positioning [16], [17], but most of them are not suitable for IoT networks. For the widely used GNSS positioning technology, it suffers severe performance degradation in dense urban and indoor environments where a large number of IoT devices may be deployed [18]. Besides, the cost of having a GNSS chip in each device may not be affordable for many low-cost IoT applications [14]. The MIMO positioning technology requires only one BS with an antenna array to perform high-accuracy 3D positioning. However, the complexity of MIMO positioning is extremely high, while most IoT devices are of limited capability, making this technology unsuitable for IoT networks. Different from the above two technologies, the OTDoA positioning is a mature multilateration technology which exploits the downlink signals of IoT networks to perform device positioning without additional hardware or complex algorithms. Thus, after careful and comprehensive consideration of various factors including positioning accuracy, technology complexity and maturity, OTDoA has been recognized as the primary positioning technology for both NB-IoT and LTE-M in 3GPP Release 14 [19]. However, in the conventional terrestrial IoT network as shown in Fig. 1(b), BSs used as anchor nodes for OTDoA positioning are relatively close in height. This poor vertical diversity of anchor nodes severely degrades the vertical accuracy of device positioning [20]. Up to now, the implementation of high-accuracy 3D positioning in IoT networks is still an unresolved issue.

In some typical vertical domains of IoT networks, both the energy efficient data collection and the high-accuracy 3D positioning are essential for enabling use cases like environment monitoring in agriculture and forestry [4], [21]. In these cases, the conventional IoT networks hardly meet the requirements due to the sparse deployment and poor vertical diversity of terrestrial BSs mentioned above. In addition, due to the high construction and maintenance costs, it is not feasible to solve these issues simply by increasing the number of BSs, especially for the applications in remote areas. Therefore, it is necessary to develop some novel IoT networks and the corresponding data collection and device positioning methods.

A. Related Work

With their high mobility and flexible deployment, UAV-based IoT platforms could be promising solutions to the above issues in existing IoT networks. UAV platforms are particularly appealing for energy efficient data collection in IoT. Compared with the fixed terrestrial BSs, UAVs are capable of flying to places where the channel conditions to selected devices are good, enabling devices to transmit data with low power or in a relatively short time [22], [23]. So, even for devices with very limited mobility, their energy consumption can be effectively reduced. Besides, UAV platforms are more likely to establish line-of-sight (LoS) communication links with IoT devices due to their relatively high altitudes [24], [25]. Potential applications of UAV platforms for IoT data collection can be roughly divided into two categories: 1). UAV-enabled IoT networks, in which single or multiple UAV platforms are used to collect data from devices [26]–[30], while terrestrial BSs are only used for backhaul links or UAV control. 2). UAV-assisted IoT networks [31]–[33], which jointly use UAV platforms and terrestrial BSs to perform data collection. In references [27]–[29], the deployment and trajectory design of UAV platforms were investigated to improve the energy efficiency of data collection in UAV-enabled IoT networks. Reference [30] proposed a method of jointly optimizing the UAV trajectory and devices' wake-up schedule to reduce energy consumption. However, in most IoT scenarios where devices have access to terrestrial BSs, the UAV-enabled IoT network is not the best choice for energy efficient data collection. For example, if there is an IoT device very close to a BS, then it is completely unnecessary to use a UAV platform to collect data from this device, because the energy consumption of data transmission from the device to the BS is already low. Thus, compared to the widely studied UAV-enabled networks, it is more practical to study the energy efficient data collection in UAV-assisted IoT networks, which is one of the objectives of our study.

In addition to being used as mobile data collectors, UAV platforms also have the potential to enhance the 3D positioning accuracy of IoT networks. UAV platforms with high-end navigation equipment like real-time kinematic (RTK) receivers have the ability to know their locations precisely [34], [35], thereby enabling them to be employed as aerial anchor nodes. Since the altitudes of UAV platforms are generally much higher than that of terrestrial BSs, the application of "UAV anchor nodes" can effectively improve the vertical diversity of anchor nodes, thereby enhancing the performance of 3D OTDoA positioning [20]. The ideas of using UAVs as aerial anchor nodes were presented in [20], [36]–[38]. The influences of UAV altitude and trajectory on positioning performance were analyzed in [36], [37]. However, these two studies mainly focused on the 2D received signal strength (RSS) positioning, which cannot meet the demands of IoT networks for 3D device positioning. In reference [38], a fully functional mini UAV system was designed for providing 3D positioning service, but it does not make full use of existing terrestrial BSs. Reference [20] studied the employment of UAVs for the enhancement of 3D positioning accuracy of cellular networks, focusing on position estimation algorithms. Up to now, the optimization of UAV trajectory and the cooperation between UAV platforms and terrestrial BSs for enhancing 3D device positioning in IoT networks have not been fully studied.

B. Main Contributions

In this paper, we propose a novel UAV-assisted IoT network which consists of a low-altitude UAV platform and multiple terrestrial BSs, and simultaneously supports the energy efficient data collection and high-accuracy 3D device positioning services. Specifically, the main contributions of this paper are summarized as follows.

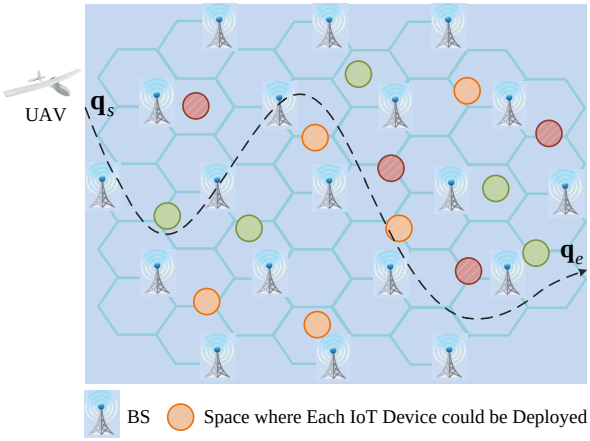

Fig. 2. The proposed UAV-assisted IoT network.

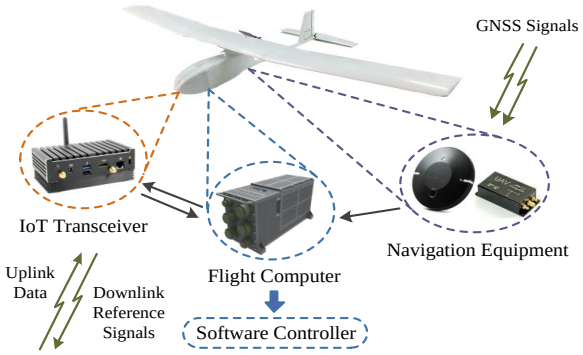

Fig. 3. Main components of the UAV platform.

- Analysis of the main challenges in conventional terrestrial IoT networks and design of a novel UAV-assisted network: In conventional IoT networks, collecting data from devices at cell edges requires high energy consumption, and the poor vertical diversity of BSs results in the unsatisfactory performance of device positioning in elevation. To overcome these challenges and enhance these two important services of IoT, we propose a UAV-assisted network, in which a UAV platform acts as both a mobile data collector and an aerial anchor node.
- Design of UAV-assisted data collection: We propose a novel data collection design for our UAV-assisted IoT network and derive the expressions for achievable transmission rates of the ground-to-ground and ground-to-air channels as well as the device's energy consumption. Simulation results demonstrate the superiority of the proposed data collection design.
- Development of a novel 3D device positioning design utilizing the UAV as an aerial anchor node to enhance the vertical positioning accuracy: We propose a design of UAV-assisted device positioning, and derive the Cramér-Rao bound (CRB) for evaluating its performance. Simulation results show that the proposed design outperforms the benchmark design using only terrestrial BSs as anchor nodes.
- Formulation of the optimization problem for implementing the energy efficient data collection and high-accuracy device positioning: We aim to minimize the maximum energy consumption of all devices by optimizing the UAV trajectory and devices' transmission schedule, while ensuring the required positioning accuracy. In particular, the uncertainty of device location is taken into account in the formulation of this problem, which has always been neglected by existing research but is very important for practical applications.
- Proposal of a DE-based method for solving this optimization problem: We divide the original mixed-integer non-convex optimization problem into three subproblems and solve them iteratively using the differential evolution (DE) algorithm. Numerical results show that the proposed method can significantly improve the energy efficiency of data collection and the accuracy of device positioning.

To the best of our knowledge, this work is the first to study both the data collection and the device positioning in a UAV-assisted IoT network.

II. System Design

In this paper, as shown in Fig. 2, we consider a UAV-assisted IoT network consisting of a low-altitude UAV platform, N terrestrial BSs and K stationary user devices. BSs and devices are denoted by sets $\mathcal{N} \triangleq \{1, 2, \cdots, N\}$ and $\mathcal{K} \triangleq \{1, 2, \cdots, K\}$, respectively. The BSs are located in a hexagonal grid with inter site distance of 500 m [39], and the user devices are uniformly dropped within the coverage of terrestrial BSs. The 3D location of each BS n is fixed and available to each device, and can be denoted by the horizontal coordinate $\mathbf{u}_n = (x_{BS,n}, y_{BS,n})^T \in \mathbb{R}^{2\times 1}$, $n \in \mathcal{N}$, and the height h_{BS}. The precise location of each device is unknown, and only sketchy information about the space where each device could be deployed is available based on devices' operation modes. At time T_0, each device k has generated sensed data of r_k bits and needs to upload it to the core network. Besides, we assume that the device location information is critical to the network due to users' requirements. Thus, in addition to uploading data, each device also needs to accurately locate itself utilizing network facilities.

The performance of data collection and device positioning services provided by BSs are unsatisfactory, especially in terms of energy efficiency and 3D positioning accuracy. Thus, in this paper, a UAV platform is used to assist BSs. The reason for using only one UAV platform is that we assume that the devices served by the proposed network do not need to frequently upload sensed data or locate themselves (perhaps only 3 to 5 times per day), which is a common assumption for most low-power IoT applications [40]. Thus, the employment of one UAV is sufficient to meet the requirements. As shown in Fig. 3, in order to support the data collection and device positioning services, the UAV platform carries three main payloads: an IoT transceiver, a flight computer and the navigation equipment. The full-featured IoT transceiver is used to collect data from IoT devices and send reference signals through the downlink channel. The navigation equipment used to obtain the real-time

precise location of the UAV platform itself could be some high-end GNSS receivers like RTK receivers. The software controller running on the flight computer maneuvers the UAV flying autonomously along a pre-determined trajectory [38], and decides the time for providing services based on the location information obtained by the navigation equipment.

The UAV flies at a fixed altitude H, and its maximum speed is $V_{\max}$. Although the transmission energy consumption could be reduced when the UAV moving up and down in height to go close to different devices, this strategy may not be desirable for the positioning service, since the continuous change in altitudes of the UAV may affect the vertical diversity. Thus, in this paper, we consider a 2D UAV trajectory at a constant altitude. In practice, the parameters H and $V_{\max}$ could be flexibly adjusted according to safety considerations and the type of UAV used (fixed-wing UAV or rotary-wing UAV). During the period from T_0 to T_0+T, the UAV platform flies from the initial location $\mathbf{q}_s \in \mathbb{R}^{2\times 1}$ to the final location $\mathbf{q}_e \in \mathbb{R}^{2\times 1}$ along a specific trajectory. Both the initial and final locations are pre-determined. We assume that the UAV platform carries enough batteries or fuel to support long-term flight missions, and the flight distance is limited primarily by its maximum speed. In order to ensure that it is feasible for the UAV to fly from $\mathbf{q}_s$ to $\mathbf{q}_e$ within T seconds, the parameters $\mathbf{q}_s$ and $\mathbf{q}_e$ should satisfy $\|\mathbf{q}_s-\mathbf{q}_e\| \le V_{\max}T$. During its flight, the UAV platform acts as a mobile data collector and aerial anchor node, together with BSs to provide data collection and 3D positioning services for devices. When the UAV arrives at the locations where it is supposed to provide services, it will wake up the corresponding IoT devices using the downlink control links and inform them to upload data or locate themselves.

In addition, since the time interval between two consecutive flight missions of the UAV platform is quite long, the prior information obtained in the previous flights, such as the previous positioning results, may not be very useful for the trajectory planning of the current flight. Thus, in the proposed network, the UAV trajectory in each flight mission is designed individually.

A. Design of UAV-Assisted Data Collection

As shown in Fig. 4, when designing the data collection process in the UAV-assisted IoT network, we consider the scenario consisting of one device, one BS and one UAV platform. Assume that the horizontal coordinate and height of the device are known and are denoted by $\mathbf{w}=(x,y)^T \in \mathbb{R}^{2\times 1}$ and h_{IoT}, respectively. This assumption will be relaxed in subsection D for the joint data collection and device positioning scenarios where the precise location of the IoT device is unknown. The projection of the UAV platform's location on the ground at time t ($t \in [T_0, T_0+T]$) is denoted by $\mathbf{q}(t) = (x_{UAV}(t), y_{UAV}(t))^T \in \mathbb{R}^{2\times 1}$. In this scenario, there are two kinds of channels that need to be analyzed, namely the ground-to-ground (G2G) channel between the device and the BS and the ground-to-air (G2A) channel between the device and the UAV platform.

Depending on the environment in which the network is located, the G2G uplink channel can be modeled as a Rayleigh

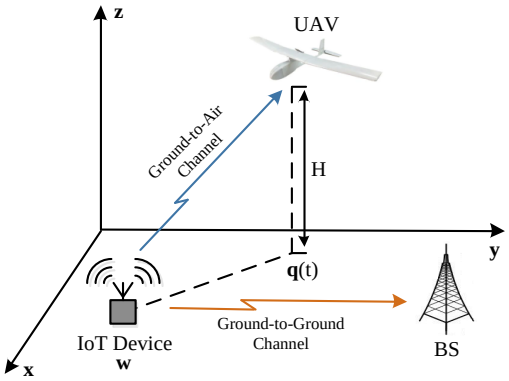

Fig. 4. UAV-assisted data collection.

(urban or suburban areas) fading channel or a Gaussian channel (rural areas). For a Rayleigh fading channel, the instantaneous channel coefficient is composed of a large-scale power attenuation (path loss) and a time-varying small-scale fading coefficient. Since the relative distance between the BS and the device remains unchanged, the path loss of the G2G channel remains constant and can be easily expressed as:

$$\begin{aligned} PL_{G2G} &= \beta_0 d_{IoT-BS}^{\alpha} \\ &= \beta_0 \left((h_{BS}-h_{IoT})^2 + \|\mathbf{u}-\mathbf{w}\|^2 \right)^{\alpha/2}, \end{aligned} \tag{1}$$

where $\beta_0 = \left(\frac{4\pi f_c}{c}\right)^2$ is the reference free space path loss at a distance of 1 m; f_c is the main frequency of the G2G channel; c is the speed of light; α is the path loss exponent (PLE). Denote the small-scale fading coefficient at time t as $\rho_{G2G}(t)$, the instantaneous capacity (bits/s) of the G2G channel is given by:

$$C_{G2G}(t) = B \cdot \log_2 \left(1 + \frac{|\rho_{G2G}(t)|^2 P}{\sigma^2 P L_{G2G}} \right), \tag{2}$$

where B is the signal bandwidth; P is the constant transmission power of the device; σ^2 is the noise power. It can be seen that the capacity of the G2G channel changes dynamically due to the time-varying nature of fading channels. As analyzed in [30], if we set some restrictions on the outage probability of the G2G channel according to practical application requirements, the achievable transmission rate of the G2G Rayleigh fading channel can be calculated in bits/s as follows:

$$\begin{aligned} R_{G2G} &= B \cdot \log_2 \left(1 + \frac{F^{-1}(\varepsilon) P}{\sigma^2 P L_{G2G}} \right) \\ &= B \cdot \log_2 \left(1 + \frac{F^{-1}(\varepsilon) P}{\sigma^2 \beta_0 \left((h_{BS}-h_{IoT})^2 + \|\mathbf{u}-\mathbf{w}\|^2 \right)^{\alpha/2}} \right), \end{aligned} \tag{3}$$

where ε is the maximum tolerable outage probability for a specific application; $F(\cdot)$ is the cumulative distribution function (CDF) of $|\rho_{G2G}(t)|^2$, and $F^{-1}(\varepsilon)$ is its inverse function. Furthermore, if the network is located in a rural area, the G2G channel is modeled as a Gaussian channel. Then, the

achievable transmission rate of the G2G Gaussian channel can be easily calculated in bits/s as follows:

$$R_{G2G} = B \cdot \log_2 \left(1 + \frac{P}{\sigma^2 \beta_0 \left(\left(h_{BS} - h_{IoT} \right)^2 + \left\| \mathbf{u} - \mathbf{w} \right\|^2 \right)^{\alpha/2}} \right). \tag{4}$$

In the UAV-assisted IoT network, the G2A channel is assumed to be dominated by the LoS component. This assumption is quite common in literature, e.g., [25], [41], because the elevation angle of the UAV platform relative to the device is typically greater than that of the BS, which results in a higher probability of a LoS communication link [23]. Therefore, only the path loss needs to be taken into consideration when analyzing the G2A channel, which can be expressed as:

$$\begin{aligned} PL_{G2A}(t) &= \beta_0 d_{IoT-UAV}^{\alpha} \\ &= \beta_0 \left(\left(H - h_{IoT} \right)^2 + \left\| \mathbf{q}(t) - \mathbf{w} \right\|^2 \right)^{\alpha/2}. \end{aligned} \tag{5}$$

Then, the achievable transmission rate (bits/s) of the G2A channel is given by:

$$\begin{aligned} R_{G2A}(t) &= B \cdot \log_2 \left(1 + \frac{P}{\sigma^2 PL_{G2A}(t)} \right) \\ &= B \cdot \log_2 \left(1 + \frac{P}{\sigma^2 \beta_0 \left(\left(H - h_{IoT} \right)^2 + \left\| \mathbf{q}(t) - \mathbf{w} \right\|^2 \right)^{\alpha/2}} \right). \end{aligned} \tag{6}$$

It is worth noting that the achievable transmission rate of the G2A channel changes dynamically over time due to the mobility of the UAV platform. For convenience, the time period T is discretized into M short time slots of length δt seconds, i.e., $T = M\delta t$. The value of the parameter δt is small enough that the UAV platform could be considered to be stationary within each time slot. Thus, in each time slot, the channel conditions and achievable transmission rates of the G2G and G2A channels are also unchanged. In the following, the horizontal coordinate of the UAV platform and the achievable transmission rates of the G2G and G2A channels in time slot m are denoted by $\mathbf{q}[m]$, $R_{G2G}[m] \triangleq R_{G2G} \cdot \delta t$ and $R_{G2A}[m] \triangleq R_{G2A}(m\delta t) \cdot \delta t$, respectively.

In this UAV-assisted network, we can control the transmission schedule of the device, including the time slots in which the device transmits its sensed data and the destination of the data transmission (BS or UAV platform). The transmission schedule of the device can be denoted by two vectors $\mathbf{x}_{BS} \in \mathbb{Z}^{1\times M}$ and $\mathbf{x}_{UAV} \in \mathbb{Z}^{1\times M}$. Setting $x_{BS}[m] = 1$ means that the device transmits its data to the BS in time slot m, while $x_{BS}[m] = 0$ means the opposite. $x_{UAV}[m]$ has a similar meaning to $x_{BS}[m]$. Since the transmission power P is constant, if the vectors $\mathbf{x}_{BS}$ and $\mathbf{x}_{UAV}$ are determined, the energy consumption of the device can be calculated as follows:

$$\theta = \sum_{m=1}^{M} \left(x_{BS}[m] + x_{UAV}[m] \right) \cdot E, \tag{7}$$

where $E \triangleq P \cdot \delta t$ is the transmission energy consumption of the device within a time slot. It is noteworthy that θ obtained by the above formula is only the energy consumption of one IoT device. As will be described in Section III below, the maximum energy consumption of all devices is regarded as the evaluation metric for the data collection service provided by the proposed network. Similarly, the amount of sensed data uploaded by the device during the time period T is given by:

$$I = \sum_{m=1}^{M} \left(x_{BS}[m] \cdot R_{G2G}[m] + x_{UAV}[m] \cdot R_{G2A}[m] \right). \tag{8}$$

In order to reduce the energy consumption, the device should choose to use the link with higher transmission rate between the G2G and G2A channels in each time slot, thereby reducing the number of time slots used for data transmission. Besides, as shown in (6), the achievable transmission rate of the G2A channel is determined by the instantaneous location of the UAV platform. Thus, the energy saving effect of data collection in the UAV-assisted IoT network is directly related to the UAV trajectory. These inferences and the superiority of our UAV-assisted data collection design will be demonstrated in Section V.A by a simulation experiment.

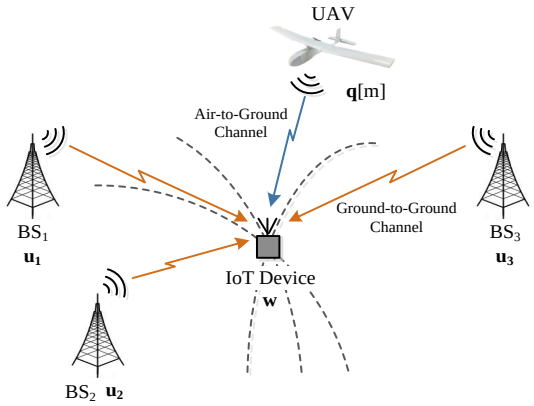

Fig. 5. UAV-assisted device positioning.

B. Design of UAV-Assisted Device Positioning

Due to its relatively low complexity and implementation cost, the OTDoA positioning technology is selected to support the device positioning service in our UAV-assisted IoT network, which is also in accordance with the current development trend of IoT networks. In OTDoA, a device measures the time-of-arrival (ToA) of reference signals from multiple time synchronized anchor nodes (BSs), and subtracts them from a ToA of a reference node to obtain the time-difference-of-arrival (TDoA) observations. As shown in Fig. 1(b), each TDoA observation corresponds to a hyperbola, and the intersection point of multiple hyperbolas is regarded as the estimate of the device's location. As mentioned above, the 3D positioning accuracy of OTDoA suffers severe degradation in conventional terrestrial IoT due to the poor vertical diversity of BSs. Thus, in this paper, the UAV platform is also employed as an aerial anchor node to improve the performance of OTDoA positioning.

Considering the scenario shown in Fig. 5, three BSs and the UAV platform are used as anchor nodes to locate a device, and

$$\sigma_{G2G}^2(\tau) = L^* \cdot \frac{\sigma^2 \beta_0 \left((h_{BS} - h_{IoT})^2 + \|\mathbf{u}_i - \mathbf{w}\|^2 \right)^{\alpha/2}}{P_{t,BS}} + \mu_{NLoS} \sigma_{NLoS}^2(\tau), \quad \mu_{NLoS} = \begin{cases} 0 & \text{LoS Scenarios} \\ 1 & \text{NLoS Scenarios} \end{cases}, \tag{15}$$

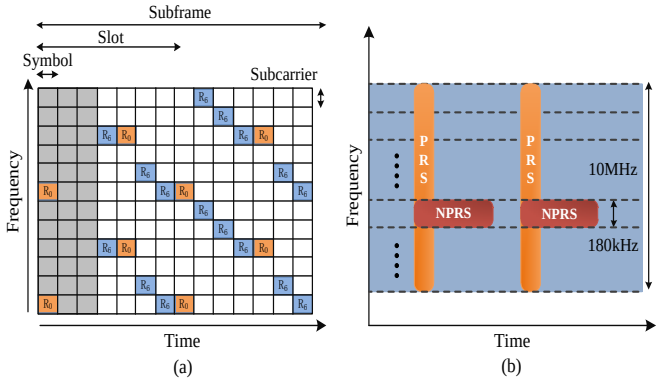

Fig. 6. (a) The allocation pattern of NPRS signal within one NB-IoT subframe (The NPRS is labeled as R_6 (blue blocks), the cell-specific reference signal (CRS) is labeled as R_0 (orange blocks)), (b) Example of PRS and NPRS transmission.

the BS 1 is the reference node. The three TDoA observations obtained by the device can be expressed as:

$$\Delta\tau_{i,1} = \tau_i - \tau_1, \qquad i = 2, 3 \text{ or UAV}, \tag{9}$$

where τ_i is the ToA of the reference signal from node i measured by the device. Then, the device itself or the IoT network can obtain the estimate of the device's location by solving the following equations:

$$\begin{aligned} c\Delta\tau_{i,1} = &\sqrt{\|\mathbf{u}_i - \mathbf{w}\|^2 + (h_{BS} - h_{IoT})^2} \\ &- \sqrt{\|\mathbf{u}_1 - \mathbf{w}\|^2 + (h_{BS} - h_{IoT})^2}, \ i = 2, 3, \end{aligned} \tag{10}$$

$$\begin{aligned} c\Delta\tau_{UAV,1} = &\sqrt{\|\mathbf{q}[m] - \mathbf{w}\|^2 + (H - h_{IoT})^2} \\ &- \sqrt{\|\mathbf{u}_1 - \mathbf{w}\|^2 + (h_{BS} - h_{IoT})^2}. \end{aligned} \tag{11}$$

In this paper, the Cramér-Rao bound (CRB), which represents the maximum achievable accuracy of device's location estimation, is used to evaluate the performance of 3D OTDoA positioning. We note that the Doppler effect caused by the relative motion between the UAV platform and IoT devices may also affect the positioning accuracy, but for this paper, we neglect this influence since there are many mature technologies can be used to estimate and compensate the Doppler frequency shift [42], [43]. To obtain the CRB for OTDoA positioning, we first analyze the performance of the ToA measurement by taking the narrowband positioning reference signal (NPRS) in NB-IoT system as an example. Similar to the PRS signal in LTE system, the NPRS is a newly defined downlink reference signal based on orthogonal frequency division multiplexing (OFDM) modulation, and is used to support OTDoA positioning in NB-IoT. The distribution of the NPRS signal in the time-frequency resource grid (RG) of an in-band deployed NB-IoT system is shown in Fig. 6(a). It can be seen that the bandwidth of the NPRS signal is 180kHz (one LTE resource block) and is much smaller than that of the LTE PRS signal, which is disadvantageous to the ToA measurement. To address this problem, the scheme of repeatedly transmitting a large number of NPRS subframes as shown in Fig. 6(b) could be adopted.

As mentioned in reference [44], the variance of the ToA measurement using any OFDM signal of length one symbol can be expressed as:

$$\sigma_{Sym}^2(\tau) = \frac{T_s^2}{8\pi^2 \cdot SNR \cdot \sum\limits_{k \in \mathcal{N}_a} p_k^2 \cdot k^2}, \tag{12}$$

where T_s and SNR are the symbol duration and signal-to-noise ratio of the received OFDM signal, respectively; $\mathcal{N}_a$ is the subset of subcarriers used to transmit reference signal; p_k is the relative power weight of each subcarrier k. Denote the subset of symbols containing NPRS signal within one subframe as $\mathcal{S}$. Then, the variance of the ToA measurement error for N_{Sub} OFDM subframes is given by:

$$\sigma_{ToA}^2(\tau) = \frac{T_s^2}{N_{Sub} \cdot 8\pi^2 \cdot SNR \cdot \sum\limits_{s \in \mathcal{S}} \sum\limits_{k \in \mathcal{N}_{s,a}} p_k^2 \cdot k^2}, \tag{13}$$

where $\mathcal{N}_{s,a}$ is the subset of subcarriers containing NPRS signal in symbol s. It is worth noting that the above formula is only applicable for LoS propagation scenarios, which mainly exist in the G2A channels in our UAV-assisted IoT network. For G2G channels, in which the multipath or NLoS propagation of signals are very common, we assume that some advanced signal processing algorithms have been employed at the IoT device to eliminate the impacts of multipath and NLoS on the ToA measurement. Without loss of generality, we model the influence of the non-ideality of the above algorithms on the ToA measurement as an additional Gaussian noise component. So, the variances of the ToA measurements for the G2A and G2G channels can be expressed as:

$$\sigma_{G2A}^2(\tau) = L^* \cdot \frac{\sigma^2 \beta_0 \left((H - h_{IoT})^2 + \|\mathbf{q}[m] - \mathbf{w}\|^2 \right)^{\alpha/2}}{P_{t,UAV}}, \tag{14}$$

where $L^* = T_s^2 \Big/ \left(N_{Sub} \cdot 8\pi^2 \sum\limits_{s \in S} \sum\limits_{k \in N_{s,a}} p_k^2 \cdot k^2 \right)$; $P_{t,UAV}$ and $P_{t,BS}$ are the transmission power of the UAV platform and terrestrial BSs, respectively. Then, the covariance matrix of the TDoA observations in (9) is given by:

$$\mathbf{R} = \begin{pmatrix} \sigma_1^2 + \sigma_2^2 & \sigma_1^2 & \sigma_1^2 \\ \sigma_1^2 & \sigma_1^2 + \sigma_3^2 & \sigma_1^2 \\ \sigma_1^2 & \sigma_1^2 & \sigma_1^2 + \sigma_{UAV}^2 \end{pmatrix}, \tag{16}$$

where σ_1^2, σ_2^2 and σ_3^2 calculated by (15) are variances of the ToA measurements corresponding to three BSs, and σ_{UAV}^2

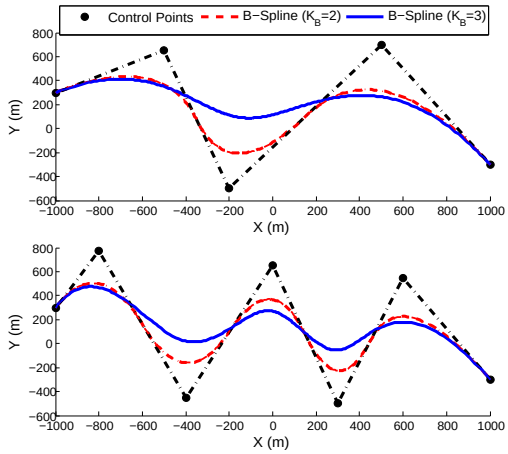

Fig. 7. B-Spline curves generated by (a) 5 or (b) 7 control points (Parameter K_B is the order of the curve).

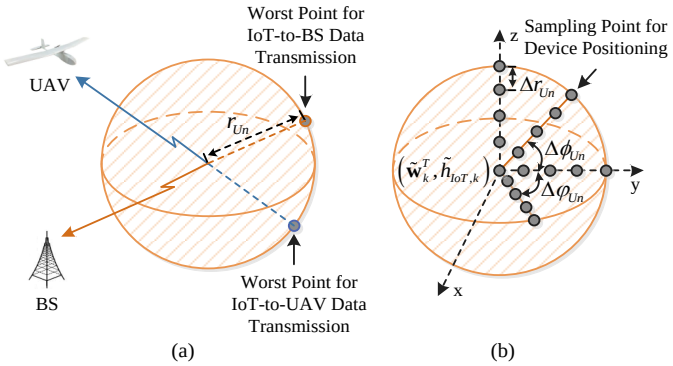

Fig. 8. Models of device location uncertainty for (a) data collection and (b) device positioning.

is calculated by (14). Finally, the CRB for 3D OTDoA positioning can be expressed as:

$$\mathrm{CRB}\left(\mathbf{q}\left[m\right]\right) = c^2 \cdot \mathrm{tr}\left(\left(\mathbf{H}^T\mathbf{R}^{-1}\mathbf{H}\right)^{-1}\right), \tag{17}$$

where $\mathbf{H}$ is the Jacobian matrix of the TDoA equations

$$\mathbf{H} = \begin{pmatrix} \frac{\partial c\Delta\tau_{2,1}}{\partial x} & \frac{\partial c\Delta\tau_{2,1}}{\partial y} & \frac{\partial c\Delta\tau_{2,1}}{\partial h_{IoT}} \\ \frac{\partial c\Delta\tau_{3,1}}{\partial x} & \frac{\partial c\Delta\tau_{3,1}}{\partial y} & \frac{\partial c\Delta\tau_{3,1}}{\partial h_{IoT}} \\ \frac{\partial c\Delta\tau_{UAV,1}}{\partial x} & \frac{\partial c\Delta\tau_{UAV,1}}{\partial y} & \frac{\partial c\Delta\tau_{UAV,1}}{\partial h_{IoT}} \end{pmatrix}, \tag{18}$$

and the expressions of $\frac{\partial c\Delta\tau_{i,1}}{\partial x}$, $\frac{\partial c\Delta\tau_{i,1}}{\partial y}$ and $\frac{\partial c\Delta\tau_{i,1}}{\partial h_{IoT}}$ are shown in [45].

It can be clearly seen from the above analysis that the performance of device positioning service in our UAV-assisted IoT network is directly related to the instantaneous location of the UAV platform when transmitting the NPRS signal. Furthermore, we assume that for an IoT device, the UAV platform only provides positioning service at the location with the best positioning performance (minimum CRB) along its trajectory. Thus, the performance of UAV-assisted device positioning depends mainly on the UAV trajectory and the geometry of BSs used for positioning, which will be studied in the following. The superiority of our UAV-assisted device positioning design will be demonstrated in Section V.B by a simulation experiment.

C. Model of UAV Trajectory

In most existing research on the applications of UAVs in IoT networks, the UAV trajectory is simply represented as a sequence of discrete waypoints connected by straight line segments. However, this kind of trajectories are only applicable for a limited number of small rotary-wing UAVs with the ability to make sharp turns during their flights. For most large rotary-wing UAVs and fixed-wing UAVs, it is unrealistic to change the flight direction instantly at each waypoint due to their relatively large turning radius. Besides, as mentioned in subsection A, the distance between any two adjacent waypoints should be small enough to ensure that the condition of the G2A channel is approximately unchanged within a time slot. So, a large number of waypoints are needed to represent a "straight line segments" type UAV trajectory, which greatly increases the complexity of trajectory design.

As shown in Fig. 7, in this paper, B-Spline curves are used to represent the UAV trajectory, which have the following advantages compared with the conventional "straight line segments" type trajectories:

- With B-Spline curves, only a few control points are needed to generate a very complicated trajectory, resulting in relatively low complexity of trajectory design and optimization.
- B-Spline curves provide at least first order derivative continuity, making them suitable as the trajectories for UAVs, especially the fixed-wing UAVs.

The specific process of generating a UAV trajectory with B-Spline curves is described in [46] and can be simplified as follows:

$$\mathbf{Q} = \mathrm{B{-}Spline}\left(\mathbf{C}\right), \tag{19}$$

where $\mathbf{Q} = \{\mathbf{q}\left[m\right], \forall m\}$ is the set of the UAV platform's locations during M time slots; $\mathbf{C} = \{\mathbf{c}_1, \mathbf{c}_2, \cdots \mathbf{c}_{N_c}\}$ ($\mathbf{c}_1 = \mathbf{q}_s, \mathbf{c}_{N_c} = \mathbf{q}_e$) is the set of the coordinates of control points. In the following, the UAV trajectory is optimized by adjusting the corresponding control points, i.e., the set $\mathbf{C}$.

D. Model of Device Location Uncertainty

In practical applications, the precise locations of IoT devices are commonly unknown before the network provides the positioning service. As described in subsections A and B, the calculation of both the achievable transmission rate for data collection and the CRB for device positioning requires the location information of devices. Thus, the uncertainty of device location inevitably affects the performance of IoT networks, but has always been neglected by existing research. In this paper, we assume that sketchy prior information about the space that each device could exist can be obtained in advance based on devices' operation modes. Then, we model the uncertain space of each device's location as a sphere with center at $\left(\tilde{\mathbf{w}}_k^T, \tilde{h}_{IoT,k}\right)$ and radius r_{Un}, as shown in Fig. 8.

It can be seen that we consider the worst cases when analyzing the impacts of device location uncertainty on the

performance of our UAV-assisted IoT network. As shown in Fig. 8(a), for data collection, we assume that the device is located at the farthest point in the sphere from the collector (BS or UAV platform), resulting in the lowest transmission rates. The reason we make this assumption is to ensure the reliability of data collection, that is, each device should complete the transmission of its data within M time slots in any case.

Since there is no closed-form expression for the CRB for 3D OTDoA positioning, the location uncertainty model for device positioning is much more complex than that for data collection. As shown in Fig. 8(b), when analyzing device positioning, we place a number of sampling points in the sphere and calculate the CRB corresponding to each of them. Then the maximum CRB obtained through the above process is treated as the performance evaluation of positioning service in the presence of device location uncertainty. This approach aims to ensure the reliability of device positioning, that is, the accuracy of 3D OTDoA positioning should meet devices' requirements even in the worst case.

III. Problem Formulation

As mentioned above, the UAV trajectory and devices' transmission schedule are two main factors affecting the performance of our UAV-assisted IoT network. In this section, to enable the energy efficient data collection and high-accuracy device positioning, the design of these two factors is formulated as an optimization problem. Our aim is to improve the energy efficiency of data collection, while ensuring the reliability of data collection and required 3D positioning performance. In a nutshell, the minimization of the maximum energy consumption of all devices is regarded as the objective function, and the 3D positioning accuracy is regarded as one of the constraints. Before modeling this problem, we first introduce the constraints used in the problem formulation as follows:

(1) Energy consumption constraint: This constraint is used to ensure that the energy consumption of each device k does not exceed θ, which is a slack variable representing the maximum energy consumption to be minimized:

$$\sum_{m=1}^{M}\left(x_{UAV}^{k}\left[m\right]+x_{BS}^{k}\left[m\right]\right)\cdot E_{k}\leq\theta,\quad\forall k. \tag{20}$$

(2) Reliable data collection constraint: This constraint ensures that the sensed data of each device is reliably collected by the IoT network within T seconds:

$$\sum_{m=1}^{M}\left(x_{UAV}^{k}\left[m\right]R_{G2A}^{k}\left[m\right]+x_{BS}^{k}\left[m\right]R_{G2G}^{k}\left[m\right]\right)\geq r_{k},\quad\forall k. \tag{21}$$

(3) Transmission scheduling constraints: In each time slot, each device could choose to simply remain silent or transmit its data to the BS or the UAV platform, but cannot simultaneously transmit to both of them. Thus, we have

$$x_{UAV}^{k}\left[m\right]\in\left\{0,1\right\},\ x_{BS}^{k}\left[m\right]\in\left\{0,1\right\},\ \forall k,m, \tag{22}$$

$$x_{UAV}^{k}\left[m\right]+x_{BS}^{k}\left[m\right]\leq1,\quad\forall k,m. \tag{23}$$

(4) Constraint on the number of devices accessing the UAV platform: Unlike BSs, the UAV platform generally cannot receive and process too much sensed data at the same time due to its limited resources and capabilities, which means that the number of devices communicating with the UAV platform in each time slot should be limited. To this end, we have

$$\sum_{k=1}^{K}\left(x_{UAV}^{k}\left[m\right]\right)\leq L,\quad\forall m, \tag{24}$$

where L is the maximum allowable number of devices accessing the UAV platform in each time slot, and can be flexibly adjusted according to users' demands and the performance of IoT communication payloads in practical implementation.

(5) Constraint on 3D positioning accuracy:

$$\min\left(\mathrm{CRB}_{k}\left(\mathbf{q}\left[m\right]\right)\right)\leq\rho_{k},\quad\forall k, \tag{25}$$

where $\mathrm{CRB}_{k}\left(\mathbf{q}\left[m\right]\right)$ is the CRB for 3D OTDoA positioning for device k in time slot m, which can be calculated by (17) and is directly related to the instantaneous location of the UAV platform $\mathbf{q}\left[m\right]$.

(6) Constraints on UAV trajectory:

$$\left\|\mathbf{q}\left[m\right]-\mathbf{q}\left[m-1\right]\right\|\leq D_{\max},\quad\forall m\geq2, \tag{26}$$

$$\mathbf{q}\left[1\right]=\mathbf{q}_{s},\ \mathbf{q}\left[M\right]=\mathbf{q}_{e}, \tag{27}$$

where $D_{\max}\triangleq V_{\max}\cdot\delta t$ is the distance that the UAV platform flies at the maximum speed for one time slot.

It is noteworthy that constraints (21) and (25) are formulated with the precise locations of IoT devices, which are commonly unavailable in practical applications. Therefore, we utilize the model of device location uncertainty introduced in Section II to rewrite these two constraints as follows:

$$\begin{aligned}\sum_{m=1}^{M}&\left(x_{UAV}^{k}\left[m\right]\mathrm{Un_{d}}\left(R_{G2A}^{k}\left[m\right]\right)\right.\\&\left.+x_{BS}^{k}\left[m\right]\mathrm{Un_{d}}\left(R_{G2G}^{k}\left[m\right]\right)\right)\geq r_{k},\ \forall k,\end{aligned} \tag{28}$$

$$\min\left(\mathrm{Un_{p}}\left(\mathrm{CRB}_{k}\left(\mathbf{q}\left[m\right]\right)\right)\right)\leq\rho_{k},\quad\forall k, \tag{29}$$

where $\mathrm{Un_{d}}\left(\cdot\right)$ and $\mathrm{Un_{p}}\left(\cdot\right)$ are two functions for dealing with the device location uncertainty in data collection and device positioning, respectively. The implementation details of these two functions are described in Section II.D and shown in Fig. 8. For both the data collection and device positioning, we focus on the worst cases in the presence of location uncertainty, so the new constraints (28) and (29) can ensure that the performance of our UAV-assisted IoT network meets the requirements.

The optimization problem of interest is formulated as follows:

$$\left(\mathrm{P1}\right):\min_{\mathbf{X},\mathbf{C},\theta}\ \theta \tag{30}$$

$$\begin{aligned}\text{s.t.}\quad&\mathrm{C1}:\ \sum_{m=1}^{M}\left(x_{UAV}^{k}\left[m\right]+x_{BS}^{k}\left[m\right]\right)\cdot E_{k}\leq\theta,\quad\forall k\\&\mathrm{C2}:\ \sum_{m=1}^{M}\left(x_{UAV}^{k}\left[m\right]\mathrm{Un_{d}}\left(R_{G2A}^{k}\left[m\right]\right)\right.\\&\qquad\left.+x_{BS}^{k}\left[m\right]\mathrm{Un_{d}}\left(R_{G2G}^{k}\left[m\right]\right)\right)\geq r_{k},\quad\forall k\\&\mathrm{C3}:\ x_{UAV}^{k}\left[m\right]\in\left\{0,1\right\},x_{BS}^{k}\left[m\right]\in\left\{0,1\right\},\quad\forall k,m\end{aligned}$$

$$\text{C4: } x_{UAV}^k[m] + x_{BS}^k[m] \le 1, \qquad \forall k, m$$
$$\text{C5: } \sum_{k=1}^{K} \left(x_{UAV}^k[m]\right) \le L, \qquad \forall m$$
$$\text{C6: } \min\left(\mathrm{Un_p}\left(\mathrm{CRB}_k\left(\mathbf{q}[m]\right)\right)\right) \le \rho_k, \qquad \forall k$$
$$\text{C7: } \mathbf{Q} = \mathrm{B{-}Spline}\left(\mathbf{C}\right)$$
$$\text{C8: } \|\mathbf{q}[m] - \mathbf{q}[m-1]\| \le D_{\max}, \qquad \forall m \ge 2$$
$$\text{C9: } \mathbf{q}[1] = \mathbf{q}_s, \mathbf{q}[M] = \mathbf{q}_e,$$

where $\mathbf{X} = \left\{\mathbf{x}_{BS}^k, \mathbf{x}_{UAV}^k, \forall k\right\}$; C1 represents the maximum data transmission power consumption of all devices; C2 is the reliability requirements for the data collection process; C3 specifies the feasible region of the optimization variable $\mathbf{X}$; C4 is the constraint that each device cannot communicate simultaneously with the BS and the UAV platform; C5 limits the number of devices accessing the UAV platform at the same time; C6 is the requirement of 3D positioning accuracy for each device k; C7 represents the process of generating the UAV trajectory utilizing a set of control points and B-Spline curves; C8 and C9 are the speed and initial/final location constraints for the UAV platform, respectively.

IV. The Proposed DE-Based Optimization Method

Due to its non-convex constraints (C2, C6 and C7) as well as the binary variable $\mathbf{X}$, the optimization problem P1 formulated in the previous section is a mixed-integer non-convex problem, which is very difficult to solve optimally. Moreover, there is no closed-form expression for the CRB used to evaluate the performance of 3D OTDoA positioning, making this problem more complicated. To find a satisfactory quasi-optimal solution, we propose an optimization method that divides the original problem into three subproblems and solves them iteratively using the differential evolution (DE) algorithm.

The proposed DE-based optimization method is summarized in Algorithm 1. The first subproblem solved by the proposed method is the selection of terrestrial BSs, in which we use a novel "fast base station selection algorithm" developed in this paper to assign each device the BSs that provide data collection and device positioning services. Then, we study the optimization of devices' transmission schedule for a given UAV trajectory, which is the second subproblem. The energy consumption corresponding to the optimal schedule is treated as the evaluation of the UAV trajectory, and is also used to construct the fitness function of the DE algorithm. Finally, in the third subproblem, the DE algorithm is used to search for the UAV trajectories with improved fitness values. Subproblems 2 and 3 are iteratively solved until the number of iterations exceeds a pre-determined threshold.

Algorithm 1 Proposed DE-Based Optimization Method

Input: Number of devices K, parameters of device location uncertainty ($\tilde{\mathbf{w}}_k$, $\tilde{h}_{IoT,k}$ and r_{Un}), maximal number of iterations $l_{\max}$, population size N_p in the DE algorithm.

Initialization:

1: Solve the subproblem of BSs selection (P2) with the proposed *fast base station selection algorithm* according to parameters $\tilde{\mathbf{w}}_k$, $\tilde{h}_{IoT,k}$ and r_{Un};
2: Randomly generate the initial population of feasible individuals $\mathbf{P}_0 \triangleq \left\{\mathbf{I}_{0,1}, \cdots, \mathbf{I}_{0,N_p}\right\}$ (each $\mathbf{I}_{0,i}$ is a control point set excluding the first and last control points) and the corresponding group of UAV trajectories $\mathbf{Q}_0 \triangleq \left\{\mathbf{Q}_{0,1}, \cdots, \mathbf{Q}_{0,N_p}\right\}$;
3: Solve the subproblem 2 (P3) to obtain the optimal transmission schedule $\mathbf{X}_{0,i}$ ($i \in \{1, \cdots, N_p\}$) and energy consumption $\theta_{0,i}$ for each UAV trajectory in $\mathbf{Q}_0$;
4: Find $i^* = \arg\min_{i \in \{1, \cdots, N_p\}} (\theta_{0,i})$; Set the best individual $\mathbf{I}^* \leftarrow \mathbf{I}_{0,i^*}$, the corresponding transmission schedule $\mathbf{X}^* \leftarrow \mathbf{X}_{0,i^*}$ and energy consumption $\theta^* \leftarrow \theta_{0,i^*}$;
5: $l \leftarrow 0$;

Repeat:

6: Solve the subproblem 3-A: Generate a trial population $\bar{\mathbf{P}}_{l+1} \triangleq \left\{\bar{\mathbf{I}}_{l+1,1}, \cdots, \bar{\mathbf{I}}_{l+1,N_p}\right\}$ and the corresponding trajectory group $\bar{\mathbf{Q}}_{l+1}$ with the *mutation* and *crossover* operations of the DE algorithm;
7: Solve the subproblem 2 (P3) to obtain $\bar{\mathbf{X}}_{l+1,i}$ and $\bar{\theta}_{l+1,i}$;
8: Solve the subproblem 3-B: Generate a new population $\mathbf{P}_{l+1}$ from $\mathbf{P}_l$ and $\bar{\mathbf{P}}_{l+1}$ with the *selection* operation of the DE algorithm, as well as $\mathbf{X}_{l+1,i}$ and $\theta_{l+1,i}$;
9: Find $i^* = \arg\min_{i \in \{1, \cdots, N_p\}} (\theta_{l+1,i})$; If $\theta_{l+1,i^*} < \theta^*$: $\mathbf{I}^* \leftarrow \mathbf{I}_{l+1,i^*}$, $\mathbf{X}^* \leftarrow \mathbf{X}_{l+1,i^*}$, $\theta^* \leftarrow \theta_{l+1,i^*}$;
10: $l \leftarrow l + 1$;

Until: $l = l_{\max}$;

Output: $\mathbf{I}^*$, $\mathbf{X}^*$ and θ^*.

A. Subproblem 1: Selection of Base Stations

In our UAV-assisted IoT network, the UAV platform cooperates with terrestrial BSs to provide services for IoT devices. As analyzed in Section II, both the achievable transmission rate of the G2G channel and the CRB for device positioning are related to the locations of BSs used, that is, the selection of the BSs used to serve each device has a influence on the network performance. Thus, at the beginning of the proposed method, we assign each device the BSs that provide data collection and device positioning services.

In our UAV-assisted data collection design described in Section II.A, except for the UAV platform, each IoT device establishes communication with only one terrestrial BS. To reduce the energy consumption, the transmission rate of the G2G channel for each device should be as large as possible, so that the sensed data could be transmitted in the shortest time with a constant power. Thus, in this subproblem, the nearest BS of each device, which commonly corresponds to the G2G channel with the highest transmission rate, is selected to provide the data collection service.

As mentioned in [45], at least four anchor nodes are required to provide 3D OTDoA positioning service for each IoT device. Moreover, the geometry of anchor nodes relative to the device can strongly affect the positioning accuracy. In our UAV-assisted device positioning design described in Section II.B, the UAV platform is innovatively employed as an aerial anchor node to enhance the performance of device positioning. Due to

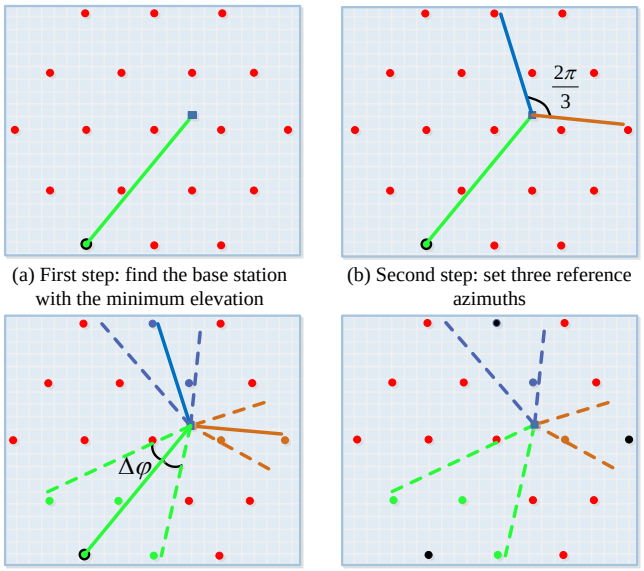

(a) First step: find the base station with the minimum elevation

(b) Second step: set three reference azimuths

(c) Third step: group the base stations

(d) Fourth step: find the subset with the minimum HDOP (black points)

Fig. 9. The proposed fast base station selection algorithm.

Algorithm 2 Fast Base Station Selection Algorithm for (P2)

Preliminary Selection:

1: Compute the elevation $\phi_{k,n}$ and azimuth $\varphi_{k,n}$ between the IoT device k and each base station n;

2: Select the BS n^* with the minimum elevation as the reference node (Fig. 9(a)), i.e., $n^* = \arg\min_{n\in\mathcal{N}} \phi_{k,n}$;

3: Set three grouping reference azimuths: $\varphi_1^* = \varphi_{k,n^*}$, $\varphi_2^* = \varphi_{k,n^*} + \frac{2\pi}{3}$ and $\varphi_3^* = \varphi_{k,n^*} + \frac{4\pi}{3}$ (Fig. 9(b));

4: Group the BSs according to the difference between the azimuth of each BS and grouping reference azimuths (Fig. 9(c)), that is, the BS n is assigned to group i ($i \in \{1,2,3\}$) if $|\varphi_{k,n} - \varphi_i^*| \le \Delta\varphi$;

5: If the number of BSs assigned to group i is zero, increase the value of $\Delta\varphi$ and regroup the BSs until there is at least one BS in each group;

Secondary Selection:

6: Select one BS from each group to form a subset and compute its corresponding HDOP. Traverse all subsets available through this approach, the subset $\mathbf{o}^*$ with minimum HDOP is assigned to the device k for positioning (Fig. 9(d)).

the relatively high altitude, the employment of the UAV platform greatly improves the vertical diversity of anchor nodes, which guarantees the vertical accuracy of device positioning. Thus, the horizontal positioning accuracy of each device is the major consideration in the selection of the terrestrial BSs for positioning. Horizontal dilution of precision (HDOP) is a powerful tool for evaluating the influence of the geometry of anchor nodes on the horizontal positioning accuracy, and a small HDOP implies satisfactory positioning performance. Therefore, when selecting the BSs for positioning, we aim to select the optimal subset corresponding to the minimum HDOP from all BSs. Furthermore, considering its extremely limited processing capability, each IoT device only uses three BSs as anchor nodes in addition to the UAV platform. Then, the selection of the BSs for positioning can be formulated as the following combinatorial optimization problem:

$$(\text{P2}): \quad \min_{\mathbf{o}} \quad \text{HDOP}\left(\mathbf{o}, \mathbf{w}_k, h_{IoT,k}\right) \qquad (31)$$
$$\text{s.t.} \quad \mathbf{o} \in \mathcal{O}.$$

where $\mathbf{o}$ is a subset consisting of three BSs used for positioning; $\mathcal{O}$ is the set containing all possible combinations of selecting 3 BSs from N BSs, i.e., $\mathcal{O} = \{\mathbf{o}_1, \mathbf{o}_2, \cdots, \mathbf{o}_G\}$, where $G = \binom{N}{3}$; $\text{HDOP}(\cdot)$ is the function for computing the HDOP corresponding to a certain subset of BSs, the expression is derived in [47]. When the number of BSs N is relatively small, the optimal solution to this problem can be easily obtained by traversing all possible subsets contained in $\mathcal{O}$. However, it is quite impractical to use the same traversal method to solve problem P2 when the number of possible subsets G is very large due to a large N. In practical applications, it is not necessary to find the optimal subset of BSs corresponding to the minimum HDOP, since there are some other subsets whose HDOPs are small enough to guarantee satisfactory horizontal positioning accuracy. Inspired by the satellite selection algorithms widely used in global navigation satellite systems (GNSSs) [48], a novel "fast base station selection algorithm" is developed in this paper to select a quasi-optimal subset for each device from a large number of BSs. The implementation process of the proposed algorithm is shown in Fig. 9 and Algorithm 2.

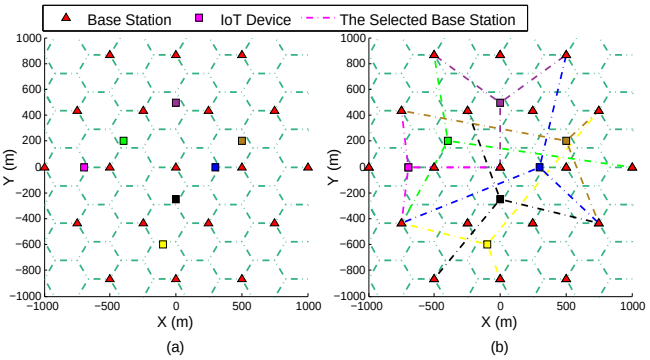

Fig. 10. An application example of the proposed fast base station selection algorithm: (a) scenario, (b) BS selection results.

We tested the proposed algorithm in a terrestrial IoT network shown in Fig. 10(a), where 19 BSs are uniformly deployed on a hexagonal grid with inter site distance (ISD) of 500 m. Our algorithm was used to select the BSs that provide positioning service for each of the 6 IoT devices at different locations, and the selection results are shown in Fig. 10(b). Intuitively, the BSs selected by our algorithm for each device are approximately evenly distributed in azimuth, which is generally considered to be beneficial for positioning. Numerically speaking, the HDOP corresponding to each selected subset of BSs does not exceed 1.5, which means that the proposed algorithm could effectively guarantee accurate horizontal positioning. It is worth noting that the

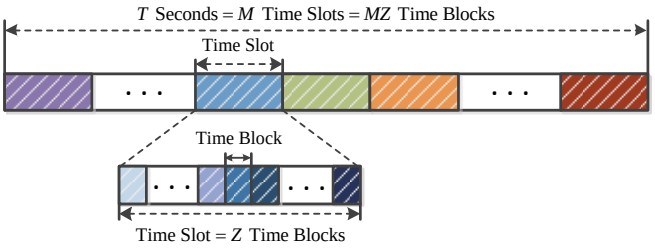

Fig. 11. Correspondence between time slots and time blocks.

precise location of each device is used in problem P2. If the device location uncertainty mentioned in Section II.D is taken into account, $\mathbf{w}_k$ and $h_{IoT,k}$ in P2 can be replaced by the coordinates of the sampling points in the sphere shown in Fig. 8(b), and the proposed algorithm is used to assign each sampling point the BSs that provide positioning service. The assignment results will be used in the subsequent procedures to calculate the CRB corresponding to each sampling point.

B. Subproblem 2: Transmission Scheduling for IoT devices

In our UAV-assisted IoT network, once the UAV trajectory is selected, the transmission schedule determines the devices' energy consumption. Thus, in this subsection, we focus on the subproblem of devices' transmission schedule optimization for a given UAV trajectory. However, the binary nature of the transmission schedule variables $\mathbf{x}_{BS}^k$ and $\mathbf{x}_{UAV}^k$ makes this subproblem quite complicated. To solve it efficiently, we modify the transmission scheduling model adopted in our network. Similar to the approach described in [30], we first divide each time slot into Z short time blocks, as shown in Fig. 11. The value of the parameter Z is large enough that $\lceil Zx \rceil \approx Zx$, where $0 \le x \le 1$ and $\lceil y \rceil$ represents the operation of rounding y up to the nearest integer. Then, the binary constraint C3 in problem P1 can be relaxed as $0 \le x_{UAV}^k[m] \le 1, 0 \le x_{BS}^k[m] \le 1, \forall k, m$, and the subproblem of devices' transmission scheduling for a given UAV trajectory can be formulated as follows:

$$\begin{aligned} (\mathrm{P3}): \quad & \min_{\mathbf{X},\theta} \quad \theta \\ & \text{s.t.} \quad \text{C3: } 0 \le x_{UAV}^k[m] \le 1, \\ & \qquad\quad 0 \le x_{BS}^k[m] \le 1, \qquad \forall k, m \\ & \qquad\quad \text{C1, C2, C4, C5.} \end{aligned} \tag{32}$$

It can be seen that the problem P3 is a standard linear programming (LP) problem, which can be easily solved by many mature software tools like CVX in Matlab. By solving this subproblem, we could obtain the minimum energy consumption corresponding to a certain trajectory, which will be used in the subsequent procedures to evaluate and optimize the UAV trajectory.

C. Subproblem 3: UAV Trajectory Optimization

As mentioned in the above subsection, for a given UAV trajectory, we can obtain its corresponding optimal transmission schedule and minimum energy consumption by solving a LP problem. In this subsection, we study how to search for a UAV trajectory with satisfactory data collection and device positioning performance, that is, the optimization of UAV trajectory. However, even if the devices' transmission schedule has been optimized in advance in problem P3, it is still very difficult to solve the remaining subproblem of UAV trajectory optimization. First of all, this subproblem is still a non-convex optimization problem due to the existence of the non-convex constraints C2 and C6. Moreover, the lack of a closed-form expression for CRB calculation in C6 means that the successive convex optimization technique used to solve non-convex trajectory optimization problems in [30], [49] is not applicable to our UAV-assisted IoT network. Thus, in this paper, we apply the differential evolution (DE) algorithm, which is one of the most popular derivative-free optimization algorithms and is suitable for solving non-convex problems, to optimize the UAV trajectory.

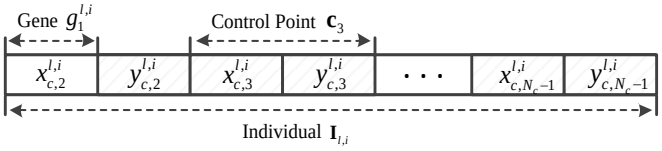

Fig. 12. Representation of individuals in the DE algorithm.

In the DE algorithm, a candidate solution of the optimization problem is called an "individual", and multiple individuals form a "population". The individuals in the population are iteratively improved by simulating the evolution and natural selection processes, so as to obtain a satisfactory solution. As mentioned in Section II.C, in this paper, a UAV trajectory is generated by a set of control points and B-Spline curves. So, when utilizing the DE algorithm to optimize the UAV trajectory, each individual $\mathbf{I}_{l,i}$ (the i-th individual in the l-th iteration) is represented by a control point set excluding the first and last control points which are fixed ($\mathbf{c}_1 = \mathbf{q}_s, \mathbf{c}_{N_c} = \mathbf{q}_e$), as shown in Fig. 12. In addition, each coordinate $x_{c,b}^{l,i}$ or $y_{c,b}^{l,i}$ ($b \in \{2, \cdots, N_c - 1\}$) in an individual is called a "gene", and the a-th gene in the i-th individual is denoted as $g_a^{l,i}$ ($a \in \{1, \cdots, 2N_c - 4\}$). The purpose of UAV trajectory optimization is to minimize the devices' energy consumption while satisfying a series of constraints, including the reliability constraint for data collection (C2), the positioning accuracy constraint (C6), as well as the constraint on the UAV platform's speed (C8). Thus, we set the fitness function used to evaluate UAV trajectories as follows:

$$fit = \frac{1}{\alpha_{Eng} f_{Eng} + \alpha_{Dat} f_{Dat} + \alpha_{Pos} f_{Pos} + \alpha_v f_v}. \tag{33}$$

It can be seen that the fitness function adopted in this subsection is the inverse of the weighted sum of four different terms, where α_X are weights and the meaning of each term is as follows: 1). f_{Eng} is the minimum energy consumption corresponding to the UAV trajectory, which is obtained by solving the problem P3. Since the DE algorithm constantly searches for the individuals with higher fitness values during its iterations, the placement of the term f_{Eng} in the denominator of the fitness function can promote the reduction of the energy

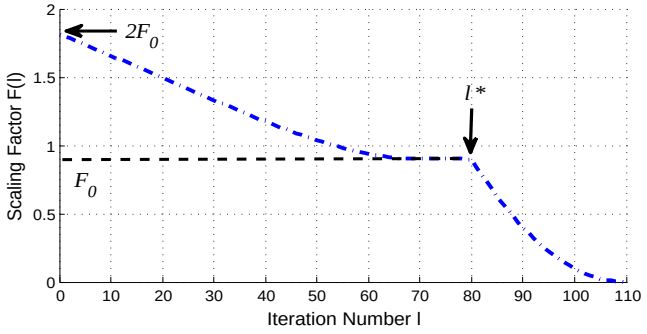

Fig. 13. Variation of the scaling factor $F(l)$ in the DE algorithm.

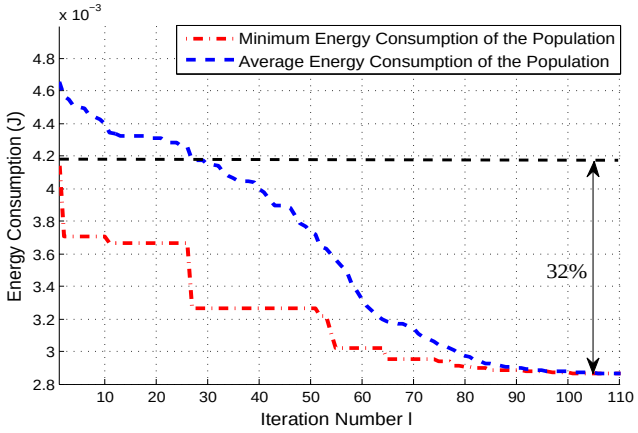

Fig. 14. Effects of using the DE algorithm to optimize the UAV trajectory.

consumption. 2). f_{Dat} is a penalty term for the constraint C2. Once a UAV trajectory fails to guarantee the reliability of the data collection service provided for each device, i.e., there is no feasible solution to the problem P3, we set $f_{Dat}=1$ and add a penalty α_{Dat} to the denominator of the fitness function, so as to reduce the fitness value of this infeasible trajectory. Similarly, 3). f_{Pos} and 4). f_v are the penalty terms for not meeting the constraints C6 and C8, respectively. Moreover, the values of weights α_{Dat}, α_{Pos} and α_v should be much larger than that of $\alpha_{Eng}f_{Eng}$, so that a UAV trajectory will be assigned a very low fitness value as long as it does not satisfy all of the constraints. With this strategy, infeasible trajectories are eliminated during the iterations of the DE algorithm, ensuring that the final optimization result is feasible.

In this subproblem of UAV trajectory optimization, N_p feasible individuals (control point sets) are randomly generated at the beginning of the DE algorithm to form the initial population $\mathbf{P}_0$, as shown in Algorithm 1. Then, three operations: mutation, crossover and selection are iteratively performed to continuously update the population and search for better individuals. In the proposed DE-based optimization method, the mutation and crossover operations are used in step 6 (subproblem 3-A) to generate a trial population $\bar{\mathbf{P}}_{l+1}$. In the mutation operation, for each individual $\mathbf{I}_{l,i}$ in the population $\mathbf{P}_l$, we generate a mutant individual $\hat{\mathbf{I}}_{l,i}$ as follows:

$$\hat{\mathbf{I}}_{l,i}=\mathbf{I}_{l,r_1}+F(l)\cdot(\mathbf{I}_{l,r_2}-\mathbf{I}_{l,r_3}), \tag{34}$$

where r_1, r_2 and r_3 are integers randomly selected from $\{1,\cdots,N_p\}$ and satisfy $r_1\neq r_2\neq r_3\neq i$; The term $(\mathbf{I}_{l,r_2}-\mathbf{I}_{l,r_3})$ is called the differential vector, which determines the direction of the mutation; $F(l)$ is a scaling factor used to control the amplification of the differential vector. Unlike existing research in which the scaling factor F is typically set to a constant $\in[0,2]$, $F(l)$ is treated as a function of the iteration number l in this paper, which can be expressed as:

$$F(l)=\begin{cases} F_0\cdot 2^{\lambda_1}, & \text{if } 0\le l\le l^* \\ F_0\cdot(1-\lambda_2)^2, & \text{otherwise,}\end{cases} \tag{35}$$

where

$$\lambda_1=\exp\left(1-\frac{l^*}{l^*-l+1}\right),\ \lambda_2=\frac{l-l^*}{l_{\max}-l^*},$$

and F_0 is a constant $\in[0,1]$; $l^*\in[0,l_{\max}]$ is the predetermined cut-off point of the piecewise-defined function $F(l)$. Fig. 13 shows the variation of the scaling factor $F(l)$ as the iteration number l increases. It can be seen that in the first segment $l\in[0,l^*]$, the value of $F(l)$ is relatively high and gradually changes from $2F_0$ to F_0, so that the DE algorithm could efficiently explore the feasible region by utilizing the mutation operation. Then, in the second segment $l\in[l^*+1,l_{\max}]$, $F(l)$ drops rapidly from F_0 to 0 within a few iterations, which promotes the convergence of the DE algorithm and the acquisition of the final optimization result. After the mutation operation, the crossover operation is applied to fuse the mutant individual $\hat{\mathbf{I}}_{l,i}$ and the corresponding original individual $\mathbf{I}_{l,i}$ to generate a trial individual $\bar{\mathbf{I}}_{l+1,i}$ according to

$$\bar{g}_a^{l+1,i}=\begin{cases}\hat{g}_a^{l,i}, & \text{if } rand(a)\le CR \text{ or } a=rnbr(i)\\ g_a^{l,i}, & \text{if } rand(a)>CR \text{ and } a\neq rnbr(i),\end{cases} \tag{36}$$

where $\bar{g}_a^{l+1,i}$ and $\hat{g}_a^{l,i}$ are the a-th genes in the trial individual $\bar{\mathbf{I}}_{l+1,i}$ and the mutant individual $\hat{\mathbf{I}}_{l,i}$, respectively; $CR\in[0,1]$ is the pre-determined crossover probability; $rand(a)$ is a uniform random number $\in[0,1]$ and $rnbr(i)$ is an integer randomly selected from $\{1,\cdots,2N_c-4\}$. Finally, after the trial population is obtained through the mutation and crossover operations, we use the selection operation to select individuals from the trial population $\bar{\mathbf{P}}_{l+1}$ and the original population $\mathbf{P}_l$ to generate a new population $\mathbf{P}_{l+1}$ for the next iteration, as mentioned in step 8 (subproblem 3-B) of Algorithm 1. In the DE algorithm, the greedy criterion is used to decide the source ($\mathbf{P}_l$ or $\bar{\mathbf{P}}_{l+1}$) of each individual in the new population, which can be expressed as:

$$\mathbf{I}_{l+1,i}=\begin{cases}\bar{\mathbf{I}}_{l+1,i}, & \text{if } fit(\bar{\mathbf{I}}_{l+1,i})\ge fit(\mathbf{I}_{l,i})\\ \mathbf{I}_{l,i}, & \text{otherwise.}\end{cases} \tag{37}$$

With this individual selection strategy, during the iterations of the DE algorithm, inferior individuals with relatively low fitness values are constantly replaced by superior individuals with high fitness values obtained through the mutation and crossover operations. After the last iteration, the individual with the highest fitness value in the population is regarded as the final optimization result. The effects of using the above

TABLE I
SIMULATION PARAMETERS

Parameter	Value
Number of time slots (M)	200
Length of time slots (δt)	2 s
Main frequency (f_c)	2.1 GHz
Signal bandwidth (B)	180 kHz
Symbol duration of the OFDM signal (T_s)	$1/(1.5\times10^4)$ s
Noise power (σ^2)	-111 dBm
Free space path loss at 1m (β_0)	38.89 dB
Path loss exponent (α)	2
Number of BSs (N)	19
Height of BSs (h_{BS})	30 m
BS layout	Hexagonal grid
Inter site distance (ISD)	500 m
Transmission power of BSs ($P_{t,BS}$)	40 dBm
UAV altitude (H)	60 m
Maximum speed of the UAV platform ($V_{\max}$)	200 m/s
Number of control points (N_c)	5
Initial location of the UAV platform ($\mathbf{q}_s$)	$(-1000,0)^T$ m
Final location of the UAV platform ($\mathbf{q}_e$)	$(1000,0)^T$ m
Maximum allowable number of devices accessing the UAV platform (L)	1
Transmission power of the UAV platform ($P_{t,UAV}$)	40 dBm
Distribution of the IoT device (horizontal)	Uniform
Distribution of the IoT device (vertical) ($\tilde{h}_{IoT,k}$)	$\mathcal{U}(10,20)$ m
Radius of location uncertainty sphere (r_{Un})	10 m
Transmission power of IoT devices (P_k)	-10 dBm
Amount of sensed data for each IoT device (r_k)	20 Mbits
Required 3D positioning CRB (ρ_k)	1 m^2
Maximal iteration number of DE algorithm ($l_{\max}$)	110
Cut-off point of the function $F(l)$ (l^*)	100
Population Size (N_p)	20
Parameter of mutation scaling factor (F_0)	0.5
Crossover probability (CR)	0.9
Weight of energy consumption term f_{Eng} in the fitness function (α_{Eng})	1
Penalty values (α_{Dat}, α_{Pos} and α_v)	0.01

DE algorithm to solve the subproblem of UAV trajectory optimization are shown in Fig. 14. It can be seen that as the iteration number increases, both the minimum and the average energy consumption of the UAV trajectory population decrease constantly. The final optimized trajectory reduces the energy consumption of our UAV-assisted IoT network by about 32% compared with the unoptimized trajectory. These phenomena demonstrate the effectiveness of the proposed DE-based optimization method.

V. NUMERICAL RESULTS

In this section, a series of simulation experiments are conducted and the corresponding numerical results are provided to verify the validity and performance of the proposed network and optimization method. First, we show the superiority of the proposed UAV-assisted data collection design over the conventional design using only terrestrial BSs via an experiment.

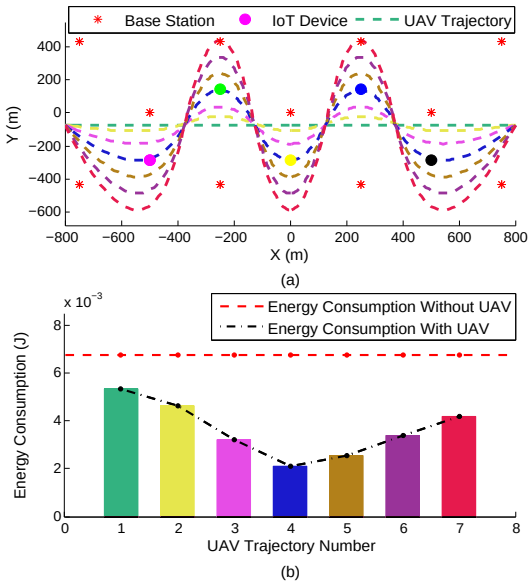

Fig. 15. Evaluation of the proposed UAV-assisted data collection design: (a) scenario, (b) devices' energy consumption.

Similarly, another experiment is conducted to prove that the proposed UAV-assisted device positioning design could bring a significant improvement in the vertical positioning accuracy. Finally, the effectiveness and superior performance of the proposed DE-based optimization method are demonstrated by two numerical simulations. Table I summarizes the key simulation parameters used in this section.

A. Evaluation of the UAV-Assisted Data Collection Design

In this subsection, we consider a UAV-assisted network consisting of a UAV platform, 11 terrestrial BSs and 5 IoT devices, as shown in Fig. 15(a). Besides, 7 different UAV trajectories are designed utilizing the B-Spline curve model mentioned in Section II.C. The devices' energy consumption of the conventional data collection design using only the terrestrial BSs and that of the proposed UAV-assisted design with different UAV trajectories are compared in Fig. 15(b). It can be seen that the energy consumption varies greatly among different designs and different trajectories, ranging from 6.7×10^{-3}J to 2.1×10^{-3}J. Obviously, the energy consumption of the proposed design is much smaller than that of the conventional design no matter which one of the 7 trajectories is adopted, and the 4th trajectory could even reduce the devices' energy consumption by 68.7%. These phenomena reflect the superiority of the proposed UAV-assisted data collection design. Moreover, from the 1st trajectory to the 7th trajectory, the distance between the UAV platform and each IoT device first decreases and then increases, and the corresponding energy consumption has the same trend. The energy consumption corresponding to the best trajectory (4th) is only 40% of that corresponding to the worst trajectory (1st). Thus, in our UAV-assisted IoT network, the UAV trajectory is one of the main factors that affects the energy efficiency. In order to prolong the lifetime of the network, it is necessary to optimize the trajectory of the UAV platform.

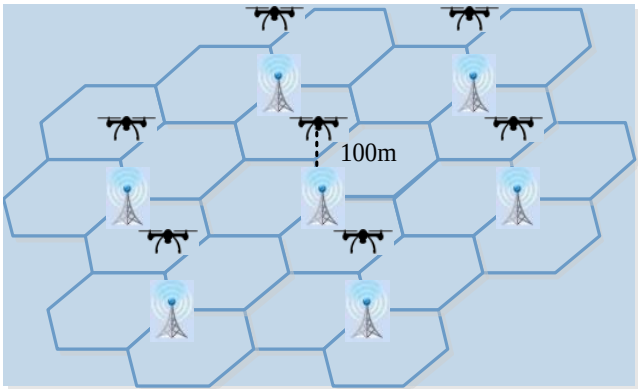

Fig. 16. Scenario of positioning performance evaluation.

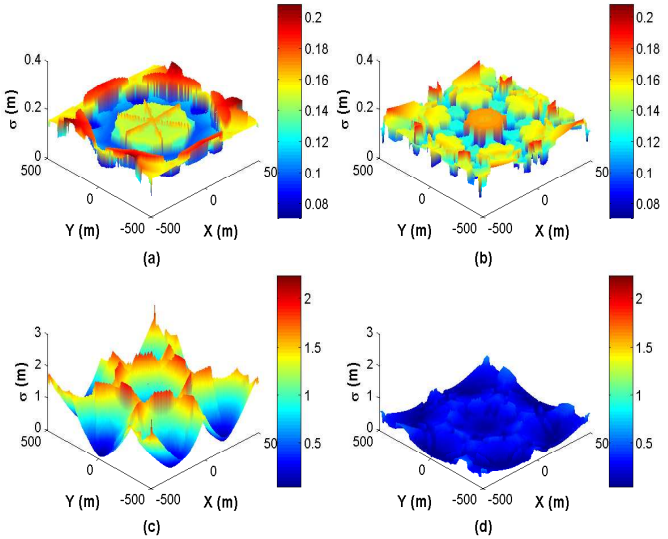

Fig. 17. Heat maps of the positioning error: the horizontal error of the (a) conventional and the (b) proposed designs, and the vertical error of the (c) conventional and the (d) proposed designs.

B. Evaluation of the UAV-Assisted Device Positioning Design

In this subsection, we compare the positioning performance of the proposed UAV-assisted device positioning design with that of the conventional design using only the terrestrial BSs. As shown in Fig. 16, we consider a scenario consisting of 7 terrestrial BSs and 7 UAV platforms, and each UAV platform is deployed 100 m above a BS. The OTDoA positioning technology described in Section II.B is used in both the conventional and proposed designs to provide 3D positioning service. We use the "heat map" method to numerically evaluate and compare the positioning performance of the two designs. When implementing this method, we first equally divide the area shown in Fig. 16 into a number of small square regions with a slide length of 10 m, and then calculate and record the standard deviation of the positioning error of the two designs while traversing each small region. After all the small regions have been traversed, the four heat maps shown in Fig. 17 can be generated based on the recorded standard deviation.

It can be seen from Fig. 17(a) and Fig. 17(b) that there is no significant difference between the horizontal positioning

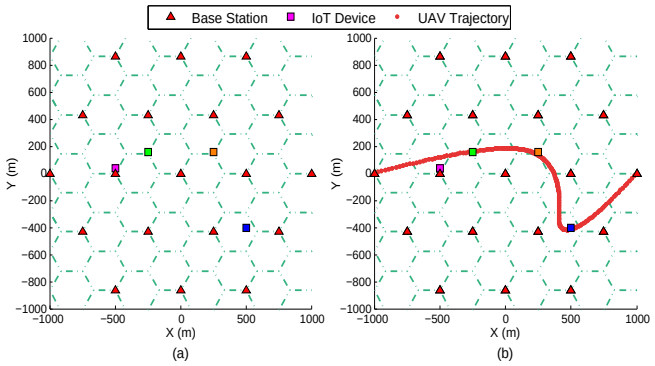

Fig. 18. Evaluation of the proposed method: (a) scenario 1, (b) optimized UAV trajectory.

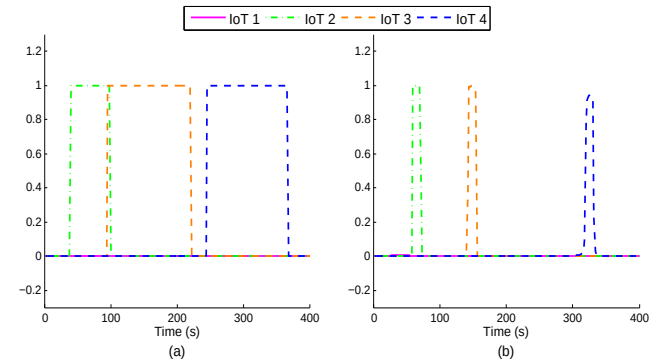

Fig. 19. Evaluation results corresponding to scenario 1: (a) comparison between the G2A and G2G channels, (b) optimized device-to-UAV transmission schedule.

accuracy of the proposed design and that of the conventional design. This is expected since the horizontal positioning accuracy in both the proposed and conventional designs is primarily determined by the geometry of the terrestrial BSs used for positioning, which has already been optimized with the proposed fast base station selection algorithm introduced in Section IV.A. However, the employment of UAV platforms greatly improves the vertical accuracy of the OTDoA positioning, as can be seen from Fig. 17(c) and Fig. 17(d). Compared with the conventional design, the proposed design reduces the range of the vertical positioning error from 2 m to 0.5 m, which means an 75% improvement in the vertical positioning accuracy. From the above numerical results, it can be concluded that the proposed UAV-assisted device positioning design could significantly improve the vertical positioning accuracy without reducing the horizontal accuracy, which is the main advantage of the proposed design.

C. Evaluation of the Proposed Method (G2G LoS Dominated)

In this subsection, the validity and performance of the proposed DE-based optimization method are first tested and evaluated in the scenario 1 shown in Fig. 18(a), where 4 IoT devices with the requirements for the data collection and 3D positioning services are considered, and the G2G channels between the devices and terrestrial BSs are modeled as LoS dominated. Fig. 18(b) and Fig. 19(b) show the optimized UAV

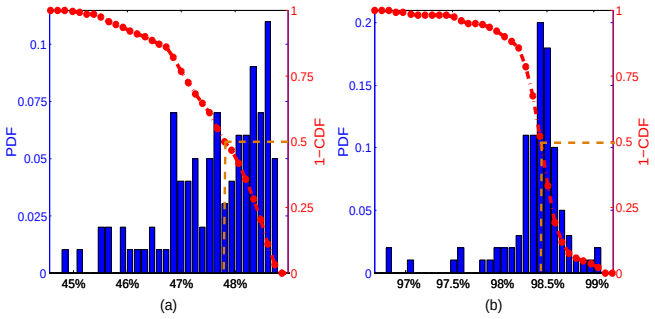

Fig. 20. Statistical results corresponding to scenario 1: (a) reduction of the energy consumption of data collection, (b) improvement of 3D positioning accuracy.

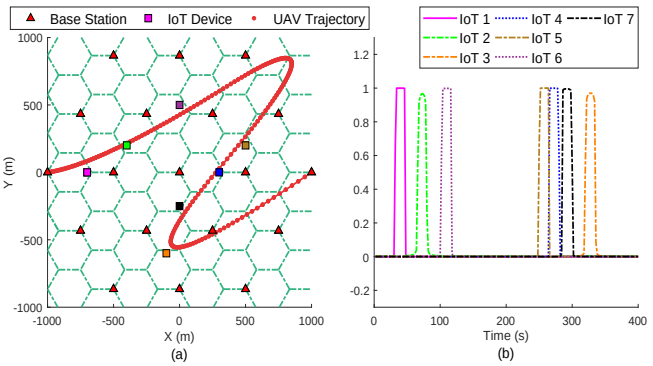

Fig. 21. Evaluation results corresponding to scenario 2: (a) scenario 2 and optimized UAV trajectory, (b) optimized device-to-UAV transmission schedule.

trajectory and devices' transmission schedule obtained by the proposed method.

Intuitively, the optimized trajectory reduces the distance between the UAV platform and each device as much as possible, thereby improving the qualities of the G2A channels. As shown in Fig. 19(a), this inference is confirmed by a comparison between the achievable transmission rates of the G2A and G2G channels, where the value of 1 indicates that the quality of the G2A channel is better than that of the G2G channel. It can be seen that the optimized UAV trajectory can make the G2A channels for three of the four devices (IoT device 2, 3 and 4) better than the corresponding G2G channels in a considerable period of time, which provides an opportunity to reduce the energy consumption of data collection. In fact, the optimized transmission schedule shown in Fig. 19(b) does take the full advantage of this opportunity, that is, it enables the devices to transmit their data to the UAV platform only for the certain period of time when the G2A channel is better than the G2G channel. It is worth noting that for device 1 in this scenario, the quality of its G2A channel is always worse than that of the G2G channel, and all its sensed data are collected by the corresponding BS. This is not surprising since device 1 is very close to a BS, so that it could transmit all its data to the BS with very low energy consumption. Thus, it is not necessary for the UAV platform to participate in the data collection process of device 1. This phenomenon reflects an advantage of the proposed UAV-assisted IoT network over the widely studied UAV-enabled networks, that is, in addition to the UAV platform, we also make full use of the existing terrestrial infrastructures. As compared with a conventional IoT network, the optimized UAV trajectory and devices' transmission schedule reduce the energy consumption of data collection by 47.88% and improve the accuracy of 3D device positioning by 98.61%.

Furthermore, Fig. 18(b) and Fig. 19(b) are the optimization results of a single simulation, which have certain randomness. In order to make the performance evaluation of the proposed method more statistically significant, we repeated this simulation 100 times and the results obtained are shown in Fig. 20. The probability density function (PDF) of the reduction of the energy consumption is shown in Fig. 20(a), where

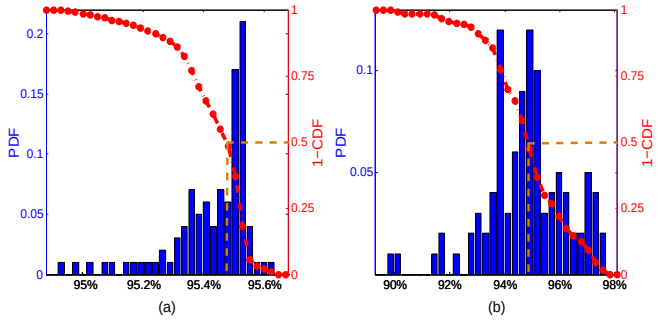

Fig. 22. Statistical results corresponding to scenario 2: (a) reduction of the energy consumption of data collection, (b) improvement of 3D positioning accuracy.

the reduction ranges from 44.83% to 48.74%. The PDF of the positioning accuracy improvement is shown in Fig. 20(b), where the improvement ranges from 96.82% to 99.04%. The functions $1-\mathrm{CDF}$ (CDF: cumulative density function) are represented by red dash-dot lines in Fig. 20(a) and (b), which can be interpreted as: the probability of reducing the energy consumption by more than 47.82% is 50%, and the probability of improving the positioning accuracy by more than 98.45% is 50%.

D. Evaluation of the Proposed Method (G2G Rayleigh Fading)

In this subsection, we consider a more practical scenario shown in Fig. 21(a), where 7 IoT devices are considered and the G2G channels are assumed to be Rayleigh fading channels. Compared with the above scenario where the G2G channels are simply modeled as LoS dominated, this scenario is more realistic for IoT networks deployed in urban or suburban environments. Here, the CDF of $\left|\rho_{G2G}\left(t\right)\right|^2$ can be expressed as $F\left(z\right) = 1 - Q_1\left(0, \sqrt{2z}\right)$, where $Q_1\left(a, b\right)$ is the Marcum Q function [50]. We set the maximum tolerable outage probability of the G2G channels to 0.01. Besides, as mentioned in Section II.B, the performance of the ToA measurement will also be degraded when the G2G channels are Rayleigh fading channels. In this scenario, the value of

$\sigma^2_{NLoS}(\tau)$ in (15) is set to 0.11 ns^2. The optimized UAV trajectory and devices' transmission schedule are shown in Fig. 21(a) and Fig. 21(b), and the statistical results are shown in Fig. 22. It can be seen that in this scenario, the proposed network and optimization method still maintain satisfactory performance. The energy consumption is reduced by about 95.48% and the positioning accuracy is improved by about 94.86%. It is noteworthy that the energy saving effect of the proposed network and method in this scenario is much better than that in the scenario 1. This is because the presence of the small-scale fading greatly reduces the achievable transmission rates of the G2G channels, thereby increasing the energy consumption of data collection in a conventional terrestrial IoT network. However, the data collection service provided by the UAV platform is not affected due to the LoS-dominated G2A channels. Thus, the employment of the UAV platform can bring more significant improvements to the energy efficiency of data collection when the G2G channels are Rayleigh fading channels.

VI. Conclusion

In this paper, a novel UAV-assisted IoT network is proposed to achieve the goal of providing energy efficient data collection and high-accuracy 3D device positioning services, in which a UAV platform is employed as a mobile data collector and aerial anchor node. Analysis and simulation show that the UAV trajectory and devices' transmission schedule are two main factors affecting the performance of the proposed network. Thus, to achieve our objectives, the design of these two factors is formulated as an optimization problem of minimizing the maximum energy consumption of all devices while ensuring the required positioning performance. The formulated problem is a mixed-integer non-convex problem, which is very difficult to solve optimally. Moreover, there is no closed-form expression for the CRB used to evaluate the 3D positioning performance. To overcome these challenges and obtain a satisfactory solution, we develop an efficient optimization method based on the differential evolution algorithm. The numerical results demonstrate that the proposed network and optimization method can significantly improve the 3D device positioning performance and lead to a notable reduction of the energy consumption of data collection. We hope that this work would provide meaningful guidance and inspiration for the development of future IoT networks, especially the air-ground integrated IoT network.

References

[1] K. Rose, S. Eldridge, and L. Chapin, "The Internet of Things: An Overview," *The Internet Society (ISOC)*, pp. 1–50, 2015.

[2] X. Li, R. Lu, X. Liang, X. Shen, J. Chen, and X. Lin, "Smart community: An internet of things application," *IEEE Communications Magazine*, vol. 49, no. 11, pp. 68–75, November 2011.

[3] L. D. Xu, W. He, and S. Li, "Internet of Things in industries: A survey," *IEEE Transactions on Industrial Informatics*, vol. 10, no. 4, pp. 2233–2243, Nov 2014.

[4] O. Elijah, T. A. Rahman, I. Orikumhi, C. Y. Leow, and M. N. Hindia, "An overview of internet of things (IoT) and data analytics in agriculture: Benefits and challenges," *IEEE Internet of Things Journal*, vol. 5, no. 5, pp. 3758–3773, Oct 2018.

[5] I. Lee and K. Lee, "The Internet of Things (IoT): Applications, investments, and challenges for enterprises," *Business Horizons*, vol. 58, no. 4, pp. 431 – 440, 2015.

[6] X. Hu, L. Yang, and W. Xiong, "A novel wireless sensor network frame for urban transportation," *IEEE Internet of Things Journal*, vol. 2, no. 6, pp. 586–595, Dec 2015.

[7] M. T. Lazarescu, "Design of a WSN platform for long-term environmental monitoring for IoT applications," *IEEE Journal on Emerging and Selected Topics in Circuits and Systems*, vol. 3, no. 1, pp. 45–54, March 2013.

[8] 3GPP TS 36.331, "Evolved Universal Terrestrial Radio Access (E-UTRA); Resource Control (RRC) Protocol Specification (Release 13)," 2016.

[9] 3GPP RP-171428, "Further NB-IoT enhancements," 2017. [Online]. Available: http://www.3gpp.org

[10] 3GPP TR 23.724, "Study on Cellular Internet of Things (IoT) support and evolution for the 5G System," v16.0.0, Dec. 2018.

[11] Yunxia Chen and Qing Zhao, "On the lifetime of wireless sensor networks," *IEEE Communications Letters*, vol. 9, no. 11, pp. 976–978, Nov 2005.

[12] C. V. Phan, Y. Park, H. H. Choi, J. Cho, and J. G. Kim, "An energy-efficient transmission strategy for wireless sensor networks," *IEEE Transactions on Consumer Electronics*, vol. 56, no. 2, pp. 597–605, May 2010.

[13] J. Rezazadeh, K. Sandrasegaran, and X. Kong, "A location-based smart shopping system with IoT technology," in *2018 IEEE 4th World Forum on Internet of Things (WF-IoT)*, Feb 2018, pp. 748–753.

[14] X. Lin, J. Bergman, F. Gunnarsson, O. Liberg, S. M. Razavi, H. S. Razaghi, H. Rydn, and Y. Sui, "Positioning for the Internet of Things: A 3GPP perspective," *IEEE Communications Magazine*, vol. 55, no. 12, pp. 179–185, Dec 2017.

[15] P. Misra and P. Enge, *Global Positioning System - signals, measurements and performance second edition*. Massachusetts: Ganga-Jamuna Press, 2006.

[16] A. Shahmansoori, G. E. Garcia, G. Destino, G. Seco-Granados, and H. Wymeersch, "5G position and orientation estimation through millimeter wave mimo," in *2015 IEEE Globecom Workshops (GC Wkshps)*, Dec 2015, pp. 1–6.

[17] K. Radnosrati, G. Hendeby, C. Fritsche, F. Gunnarsson, and F. Gustafsson, "Performance of OTDOA positioning in narrowband IoT systems," in *2017 IEEE 28th Annual International Symposium on Personal, Indoor, and Mobile Radio Communications (PIMRC)*, Oct 2017, pp. 1–7.

[18] A. Dammann, R. Raulefs, and S. Zhang, "On prospects of positioning in 5G," in *2015 IEEE International Conference on Communication Workshop (ICCW)*, June 2015, pp. 1207–1213.

[19] A. Hoglund, X. Lin, O. Liberg, A. Behravan, E. A. Yavuz, M. Van Der Zee, Y. Sui, T. Tirronen, A. Ratilainen, and D. Eriksson, "Overview of 3GPP release 14 enhanced NB-IoT," *IEEE Network*, vol. 31, no. 6, pp. 16–22, November 2017.

[20] J. Khalife, K. Shamaei, S. Bhattacharya, and Z. Kassas, "Centimeter-accurate UAV navigation with cellular signals," in *Proceedings of ION GNSS Conference*, 2018.

[21] S. Dhingra, R. B. Madda, A. H. Gandomi, R. Patan, and M. Daneshmand, "Internet of things mobile-air pollution monitoring system (iot-mobair)," *IEEE Internet of Things Journal*, vol. 6, no. 3, pp. 5577–5584, June 2019.

[22] Y. Zeng, R. Zhang, and T. J. Lim, "Wireless communications with unmanned aerial vehicles: opportunities and challenges," *IEEE Communications Magazine*, vol. 54, no. 5, pp. 36–42, May 2016.

[23] S. Zhang, Y. Zeng, and R. Zhang, "Cellular-enabled uav communication: A connectivity-constrained trajectory optimization perspective," *IEEE Transactions on Communications*, vol. 67, no. 3, pp. 2580–2604, March 2019.

[24] A. Al-Hourani, S. Kandeepan, and A. Jamalipour, "Modeling air-to-ground path loss for low altitude platforms in urban environments," in *2014 IEEE Global Communications Conference*, Dec 2014, pp. 2898–2904.

[25] W. Khawaja, I. Guvenc, D. W. Matolak, U. Fiebig, and N. Schneckenburger, "A survey of air-to-ground propagation channel modeling for unmanned aerial vehicles," *IEEE Communications Surveys Tutorials*, vol. 21, no. 3, pp. 2361–2391, thirdquarter 2019.

[26] X. Ma, R. Kacimi, and R. Dhaou, "Fairness-aware UAV-assisted data collection in mobile wireless sensor networks," in *2016 International Wireless Communications and Mobile Computing Conference (IWCMC)*, Sep. 2016, pp. 995–1001.

[27] M. Mozaffari, W. Saad, M. Bennis, and M. Debbah, "Mobile internet of things: Can uavs provide an energy-efficient mobile architecture?"

in *2016 IEEE Global Communications Conference (GLOBECOM)*, Dec 2016, pp. 1–6.

[28] D. Yang, Q. Wu, Y. Zeng, and R. Zhang, "Energy tradeoff in ground-to-uav communication via trajectory design," *IEEE Transactions on Vehicular Technology*, vol. 67, no. 7, pp. 6721–6726, July 2018.

[29] M. Mozaffari, W. Saad, M. Bennis, and M. Debbah, "Mobile unmanned aerial vehicles (uavs) for energy-efficient internet of things communications," *IEEE Transactions on Wireless Communications*, vol. 16, no. 11, pp. 7574–7589, Nov 2017.

[30] C. Zhan, Y. Zeng, and R. Zhang, "Energy-efficient data collection in uav enabled wireless sensor network," *IEEE Wireless Communications Letters*, vol. 7, no. 3, pp. 328–331, June 2018.

[31] I. Bor-Yaliniz and H. Yanikomeroglu, "The new frontier in RAN heterogeneity: Multi-tier drone-cells," *IEEE Communications Magazine*, vol. 54, no. 11, pp. 48–55, November 2016.

[32] S. Sekander, H. Tabassum, and E. Hossain, "Multi-tier drone architecture for 5G/B5G cellular networks: Challenges, trends, and prospects," *IEEE Communications Magazine*, vol. 56, no. 3, pp. 96–103, March 2018.

[33] J. Lyu, Y. Zeng, and R. Zhang, "UAV-aided offloading for cellular hotspot," *IEEE Transactions on Wireless Communications*, vol. 17, no. 6, pp. 3988–4001, June 2018.

[34] W. Stempfhuber and M. Buchholz, "A precise, low-cost RTK GNSS system for UAV applications," in *roc. of Unmanned Aerial Vehicle in Geomatics, ISPRS*, 2011, pp. 289–293.

[35] Z. Liu, Z. Li, B. Liu, X. Fu, I. Raptis, and K. Ren, "Rise of mini-drones: Applications and issues," in *Proceedings of the 2015 Workshop on Privacy-Aware Mobile Computing*, ser. PAMCO '15. New York, NY, USA: ACM, 2015, pp. 7–12.

[36] H. Sallouha, M. M. Azari, A. Chiumento, and S. Pollin, "Aerial anchors positioning for reliable RSS-based outdoor localization in urban environments," *IEEE Wireless Communications Letters*, vol. 7, no. 3, pp. 376–379, June 2018.

[37] H. Sallouha, M. M. Azari, and S. Pollin, "Energy-constrained UAV trajectory design for ground node localization," in *2018 IEEE Global Communications Conference (GLOBECOM)*, Dec 2018, pp. 1–7.

[38] Z. Liu, Y. Chen, B. Liu, C. Cao, and X. Fu, "HAWK: An unmanned mini-helicopter-based aerial wireless kit for localization," *IEEE Transactions on Mobile Computing*, vol. 13, no. 2, pp. 287–298, Feb 2014.

[39] 3GPP TR 38.901, "Study on channel model for frequencies from 0.5 to 100 GHz," v15.0.0, Jun. 2018.

[40] 3GPP TR 45.820, "Cellular system support for ultra-low complexity and low throughput Internet of Things (CIoT)," v13.1.0, Nov. 2015.

[41] B. Li, Z. Fei, and Y. Zhang, "UAV communications for 5G and beyond: Recent advances and future trends," *IEEE Internet of Things Journal*, vol. 6, no. 2, pp. 2241–2263, April 2019.

[42] D. Oh and J. Lee, "Robust super-resolution TOA estimation against Doppler shift for vehicle tracking," *IEEE Communications Letters*, vol. 18, no. 5, pp. 745–748, May 2014.

[43] Z. Hou, Y. Zhou, L. Tian, J. Shi, Y. Li, and B. Vucetic, "Radio environment map-aided Doppler shift estimation in LTE railway," *IEEE Transactions on Vehicular Technology*, vol. 66, no. 5, pp. 4462–4467, May 2017.

[44] J. A. del Peral-Rosado, J. A. López-Salcedo, G. Seco-Granados, F. Zanier, and M. Crisci, "Achievable localization accuracy of the positioning reference signal of 3GPP LTE," in *2012 International Conference on Localization and GNSS*, June 2012, pp. 1–6.

[45] C. Chen and W. Wu, "Three-dimensional positioning for LTE systems," *IEEE Transactions on Vehicular Technology*, vol. 66, no. 4, pp. 3220–3234, April 2017.

[46] I. K. Nikolos, K. P. Valavanis, N. C. Tsourveloudis, and A. N. Kostaras, "Evolutionary algorithm based offline/online path planner for UAV navigation," *IEEE Transactions on Systems, Man, and Cybernetics, Part B (Cybernetics)*, vol. 33, no. 6, pp. 898–912, Dec 2003.

[47] J. A. Del Peral-Rosado, R. E. I Castillo, J. Miguez-Sanchez, M. Navarro-Gallardo, J. A. Garcia-Molina, J. A. López-Salcedo, G. Seco-Granados, F. Zanier, and M. Crisci, "Performance analysis of hybrid GNSS and LTE localization in urban scenarios," in *2016 8th ESA Workshop on Satellite Navigation Technologies and European Workshop on GNSS Signals and Signal Processing (NAVITEC)*, Dec 2016, pp. 1–8.

[48] M. Zhang and J. Zhang, "A fast satellite selection algorithm: Beyond four satellites," *IEEE Journal of Selected Topics in Signal Processing*, vol. 3, no. 5, pp. 740–747, Oct 2009.

[49] A. Li, Q. Wu, and R. Zhang, "UAV-enabled cooperative jamming for improving secrecy of ground wiretap channel," *IEEE Wireless Communications Letters*, vol. 8, no. 1, pp. 181–184, Feb 2019.

[50] F. Ono, H. Ochiai, and R. Miura, "A wireless relay network based on unmanned aircraft system with rate optimization," *IEEE Transactions on Wireless Communications*, vol. 15, no. 11, pp. 7699–7708, Nov 2016.